

Award Accounts

The Chemical Society of Japan Award for Young Chemists for 2002

Novel π-Conjugated Nano-Supramolecules Having Fine-Controlled Metal-Assembling Functions

Masayoshi Higuchi and Kimihisa Yamamoto*

Kanagawa Academy of Science & Technology (KAST), and Department of Chemistry, Faculty of Science & Technology, Keio University, Yokohama 223-8522

Received September 10, 2003; E-mail: yamamoto@chem.keio.ac.jp

Dendritic and cyclic polyphenylazomethines (DPA and CPA) were exploited as π-conjugated polymer ligands having novel topological structures. DPAs were synthesized by the convergent method via dehydration in the presence of $TiCl_4$. DPA G4 molecules have a sphere-like structure with a 2.3-nm diameter, and they are regularly assembled without deformation of the molecule on a plate, as observed by means of GPC, molecular modeling, TEM, AFM, and π–*A* measurements. The stepwise radial complexation in DPAs with $SnCl_2$ was observed as a stepwise shift in the isosbestic point in the UV–vis spectra; this conclusion was further supported by TEM, NMR, and shell-selective reduction (SSR) of the imines. The order of complexation among the shells permits control by the introduction of electron-withdrawing groups to the DPA structure. CPA*n*-ab and CPA*n*-aabb (designated as CPAX-Y where X and Y are the degree of polymerization and whether the polymerization was AB- or AABB-type, respectively) was synthesized via dehydration in the presence of $TiCl_4$, $TiCl_4(THF)_2$ or *p*-toluenesulfonic acid (PTS). The unique structures of CPA*n*-ab and CPA*n*-aabb: triangle, square, or oblong, and their regular molecular-packing were revealed by NMR, MD calculations, and X-ray crystal analysis. CPA*n*-aabb shows reversible redox functions by protic acid doping, unlike conventional polyphenylazomethine (PPA).

Organic–metallic hybrid nano-materials[1] have received much attention for use in electronic, photonic, or magnetic nano-devices, or catalysts, because chemical or electrochemical interactions amplified by fine-controlled-blending of organic materials and metal ions/clusters are expected to enhance their properties and cause novel functions. π-Conjugated polymers, which have excellent redox properties and unique chromic functions, are especially attractive organic components in the hybrid nano-matrials.[2,3] For example, polyaniline and polypyrrole, which are representative π-conjugated polymers having coordination sites, show redox-activity by complexation with metal ions such as copper, iron, or palladium, and the polymer complexes work as efficient oxidation catalysts under oxygen atmosphere based on the electrochemical interaction between their π-conjugated polymers and the metal ions.[4] For the development of organic–metallic hybrid nano-materials, it is essential to control the number and position of the metal ions in the polymer complexes, but this is quite difficult when using linear polymers. Because the conventional linear polymers have a "spaghetti-like" flexible structure with various molecular weights, metal ions are randomly complexed with the coordination sites of the polymers (Fig. 1). In order to solve this problem, we focused on polymeric ligands having novel topologies such as dendrimers and macrocycles with a single molecular weight and a single structure. Their clearly-defined structures should enable both precise metal-assembling inside the polymers and regular polymer-assembling, which is important for constructing nano-devices (Fig. 1).

Dendrimers[5] are perfectly branched polymers with successive shells of branch units surrounding a central core; they were first defined and synthesized by Tomalia. Their tree-like topologies cause gradients in the branch density from the interior to the exterior, which direct the transfer of charge and energy from the dendrimer periphery to its core.[6] In addition, dendrimers having coordination sites can trap many metal ions or metal clusters within the voids in the dendrimers.[7] Therefore, dendrimers are attractive organic polymers in organic–metallic hybrid materials. For example, Crooks et al have reported preparation of metal clusters in poly(amidoamine) (PAMAM) dendrimers and their unique catalytic properties.[7c] However, the precise metal-assembling using the conventional dendrimers such as PAMAM dendrimers is difficult and has not been reported yet. On the other hand, macrocycles[8] are also important polymers for host–guest chemistry, and a precise collection of plural metal ions is expected based on their clearly-defined structures. However, in general, syntheses of macrocycles are not easy because of their low yields and difficult isolation. One way to solve these problems is considered to be introduction of a novel π-conjugated backbone to dendritic and macrocyclic structures by exploiting novel synthetic methods.

Among π-conjugated polymers, we selected polyphenylazomethines (PPA)[9] as the backbone for the novel topological

Published on the web May 6, 2004; DOI 10.1246/bcsj.77.853

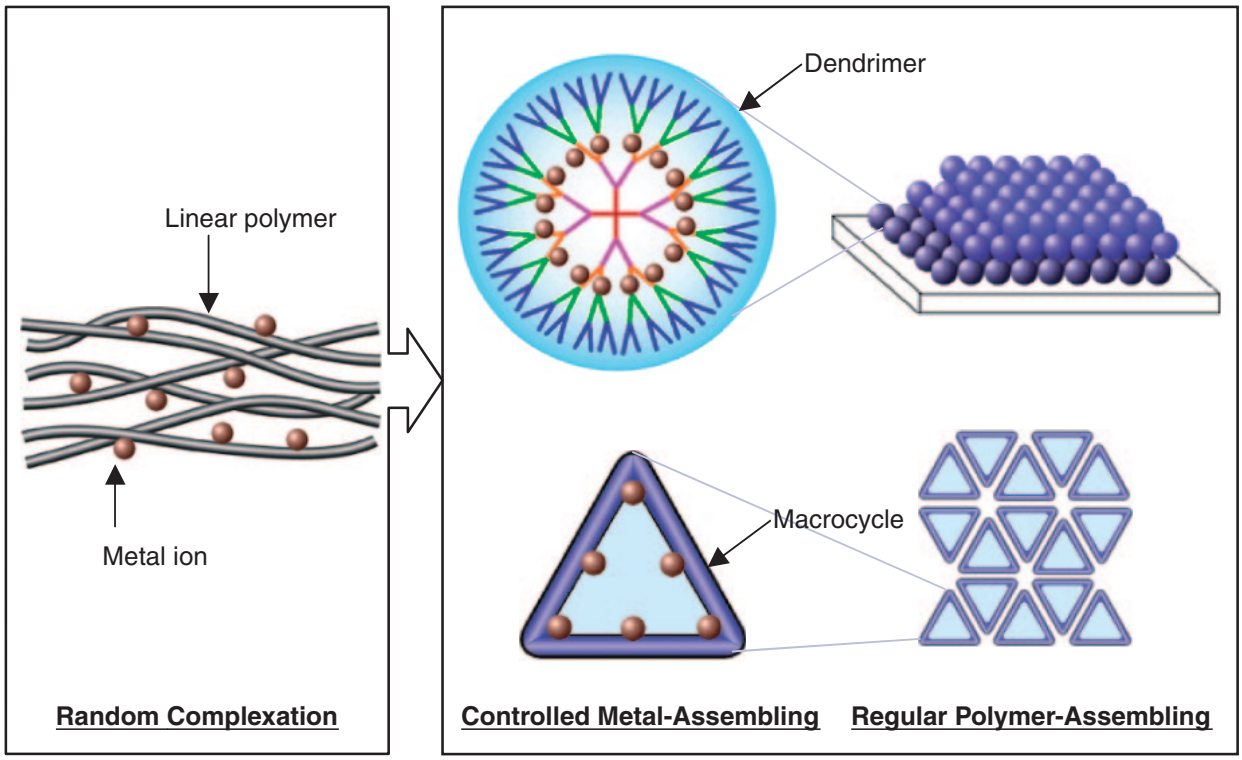

Fig. 1. Creation of dendritic and macrocyclic π-conjugated polymer ligands for achievement of controlled metal-assembling in the polymers and the regular polymer-assembling.

structures, because many coordination site of PPA are attractive for constructing novel hybrid materials. In addition, PPA is a π-conjugated polymer with high thermal stability, good mechanical strength, meltability, and fiber-forming properties, and is relatively easily synthesized via dehydration of aromatic aldehydes/ketones with aromatic amines. On the other hand, their insolubility in organic solvents limits their processing and makes it difficult to understand their structures and the complexation behavior with metal ions. However, we expected that introduction of novel topological structures enhances their solubilities due to the decrease in molecular stacking.

We herein describe the syntheses of novel π-conjugated nano-supramolecules, dendritic polyphenylazomethines[10] (DPA) and cyclic polyphenylazomethines[11] (CPA), and their structures, controlled metal-assembling, regular polymer-assembling, and electrochemical properties.

1. Dendritic Polyphenylazomethines

1.1 Synthesis, Solubility, and Thermal Stability. In the dehydration of aldehydes/ketones with amines, the addition of an acid is sometimes necessary to enhance the electrophilicity of the carbonyl carbon. *p*-Toluenesulfonic acid (PTS) is often used as an efficient catalyst in the synthesis of polyphenylazomethines via the dehydration of amines with *aldehydes*.[12] However, PTS is not an efficient catalyst in the dehydration of aromatic amines with *aromatic ketones*, because the electrophilicity of the carbonyl carbon in the aromatic ketones is much lower than that in aldehydes (Scheme 1, Run 1). On the other hand, $TiCl_4$ is a strong Lewis acid and was revealed to act as an effective dehydration agent (Run 2). This dehydration is known to proceed via metathesis of benzophenone with a

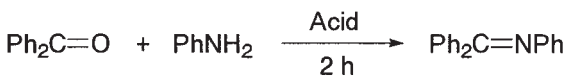

Run	Acid (equiv.)	Solv.	Temp., °C	Yield, %
1	PTS (0.10)	*p*-Xylene	140	19
2	$TiCl_4$ (0.75)	PhCl	125	91

Scheme 1. Formation of an imine bond.

Ti=N compound, which is formed by the reaction of aniline with $TiCl_4$. In addition, PTS is not suitable in such multistep syntheses for dendrimer preparation, because the readily-formed imine bonds can be hydrolyzed due to an equilibrium reaction, while $TiCl_4$ is a good agent for this synthesis, because the dehydration using $TiCl_4$ is irreversible.

Dendritic polyphenylazomethines (DPA G1, G2, G3, and G4, designated as GX, where X is the generation number) were synthesized by the convergent method (Scheme 2). DPA dendron G2 was formed via the dehydration of benzophenone with 4,4′-diaminobenzophenone (**1**) in the presence of $TiCl_4$ and 1,4-diazabicyclo[2.2.2]octane (DABCO) and was isolated by silica gel column chromatography in 48% yield. A large excess of benzophenone for **1** was used in this reaction in order to prevent undesirable dehydration between two molecules of **1**, which lowers the yield of the dendron. Similarly, DPA dendrons G3 and G4 were obtained in 64 and 20% yields by dehydration of the dendrons G2 and G3 with **1**, respectively. DPAs G1–4 were synthesized by dehydration of benzophenone, the

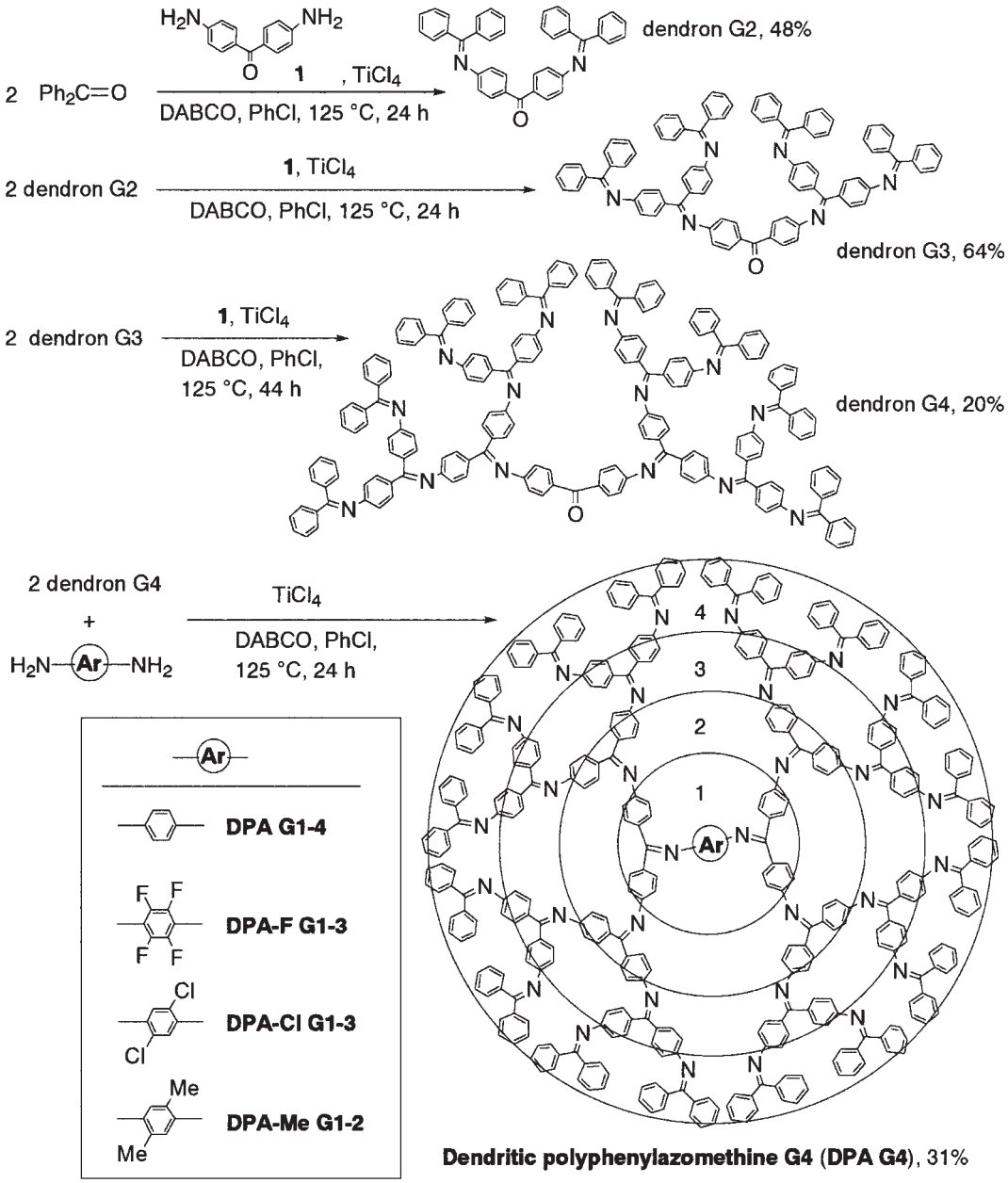

Scheme 2. Convergent synthesis of dendritic polyphenylazomethines (DPA).

dendrons G2, G3, and G4 with *p*-phenylenediamine and were isolated in 91, 62, 45, and 31% yields, respectively. DPAs and the dendrons were identified as a single molecule by MS, NMR, IR, GPC, and elemental analysis (Fig. 2), and the absence of Ti in DPAs was confirmed by ICP–MS (the concentration of Ti in the DPA G4 powder: under 0.1 ppm).

Linear polyphenylazomethines (PPA) have very poor solubility, but DPAs show high solubility for the common solvents such as chloroform, THF, or DMSO because of weak π-stacking between the bulky DPA molecules. The high solubility enabled the structural studies, investigating the complexation behavior, and the polymer assembling on a plate, as will be described later. In addition, DPAs showed high thermal stabilities similar to those of PPA based on the strong imine bond with large bond energy (615 kJ/mol); the temperatures for a 10% weight loss ($Td_{10\%}$) of DPA G2–4 were 514, 511, and 521 °C, respectively ($Td_{10\%}$ of PPA: 507 °C), which is a favorable property for actual applications.

1.2 Molecular Structure (X-Ray Crystal Analysis and Molecular Modeling). Crystals of DPA G2 were obtained by slow vapor diffusion of methanol into a chlorobenzene solution of DPA G2, and the molecular structure was determined by X-ray crystal analysis (Fig. 3). The following three types of important information about the structure of DPA were obtained. (1) DPA G2 has a centrosymmetrical structure; (2) conformational patterns among the three phenyl-rings connected to the imines were observed as follows. Phenyl rings connected to nitrogen of the imines (*N*-connected phenyl rings) are perpendicular to the imine bond (C12–C11–N2–C14 angle: −88.0(5)°), and the angle is twisted about 30–40° by steric hindrance (C31–C30–N3–C33 angle: 64.8(5)°; C4–C6–N1–C7 angle: 51.7(5)°). In the two phenyl rings connected to carbon of the

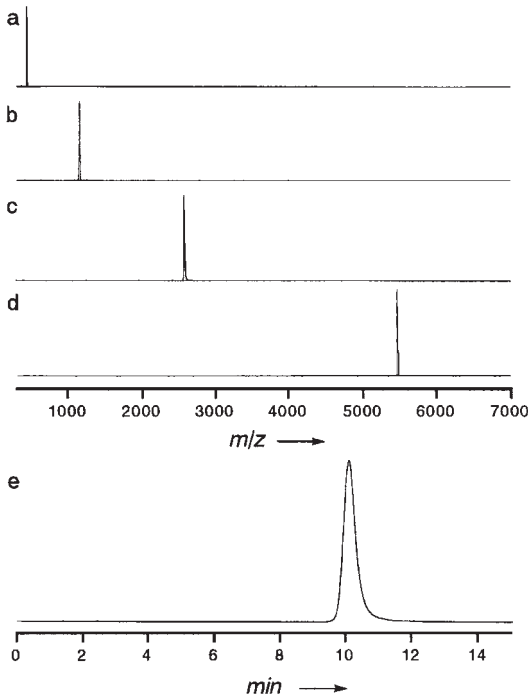

Fig. 2. (a–d) MALDI-TOF-MS spectrum of DPA G1–4 (DPA G4: calcd 5451.26 $[M + H]^+$, found 5451.48) and (e) GPC trace of DPA G4 ($M_w/M_n = 1.02$).

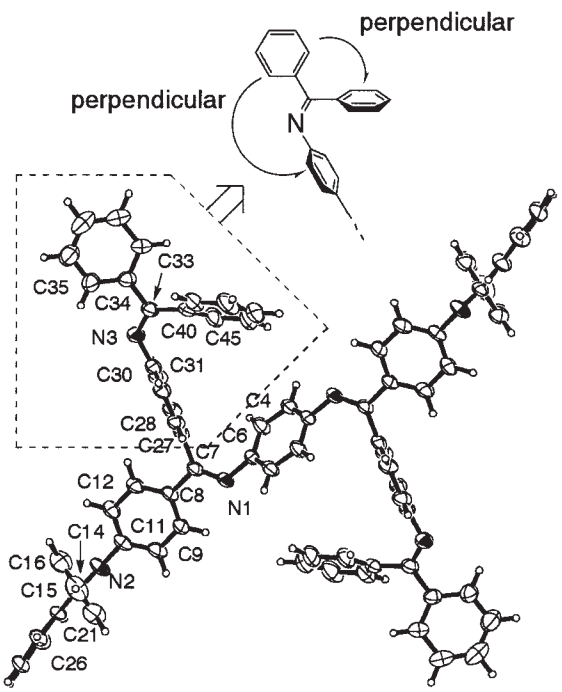

Fig. 3. ORTEP drawing of DPA G2 with 30% ellipsoid.

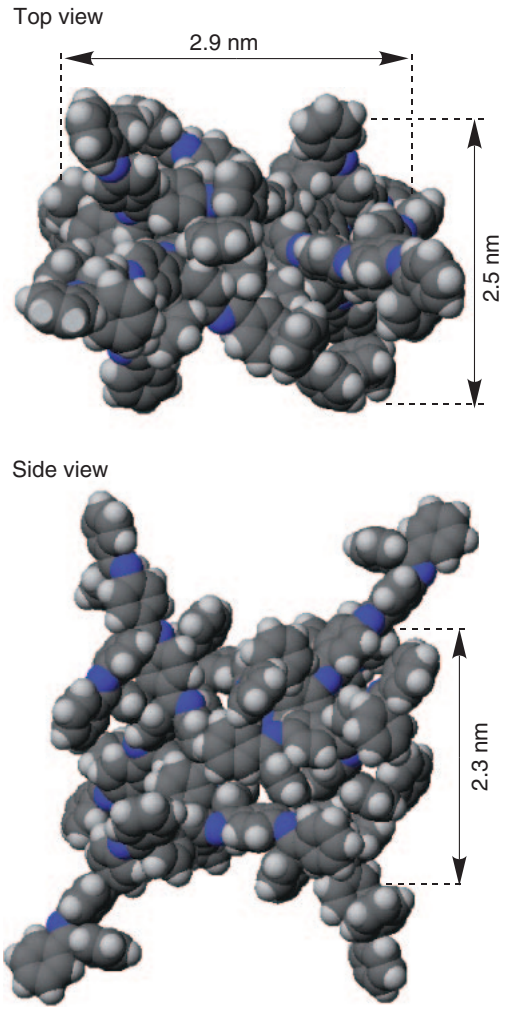

Fig. 4. Molecular model of DPA G4 based on the crystal structure of DPA G2 (Fig. 3).

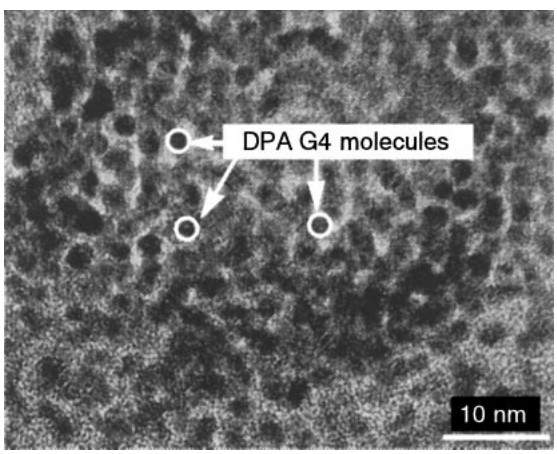

Fig. 5. TEM picture of DPA G4.

imines (*C*-connected phenyl rings), the *trans* ones for the *N*-connected phenyl ring are parallel to the imine bond (N1–C7–C8–C9 angle: −7.2(5)°; N2–C14–C21–C26 angle: −3.6(6)°), and the angle is twisted about 30° by steric hindrance (N3–C33–C34–C35 angle: 26.4(6)°). On the other hand, the *cis* *C*-connected phenyl rings are rather perpendicular to the imine bond (N1–C7–C27–C28 angle: 117.3(4)°; N2–C14–C15–C16 angle: 75.4(5)°; N3–C33–C40–C45 angle: 50.5(6)°). (3) The *cis* *C*-connected phenyl rings at the terminals of the dendritic branch elongate toward the *inside* of the dendrimer. According to the conformational rules, molecular modeling of DPA G4 was performed (Fig. 4). With increasing gener-

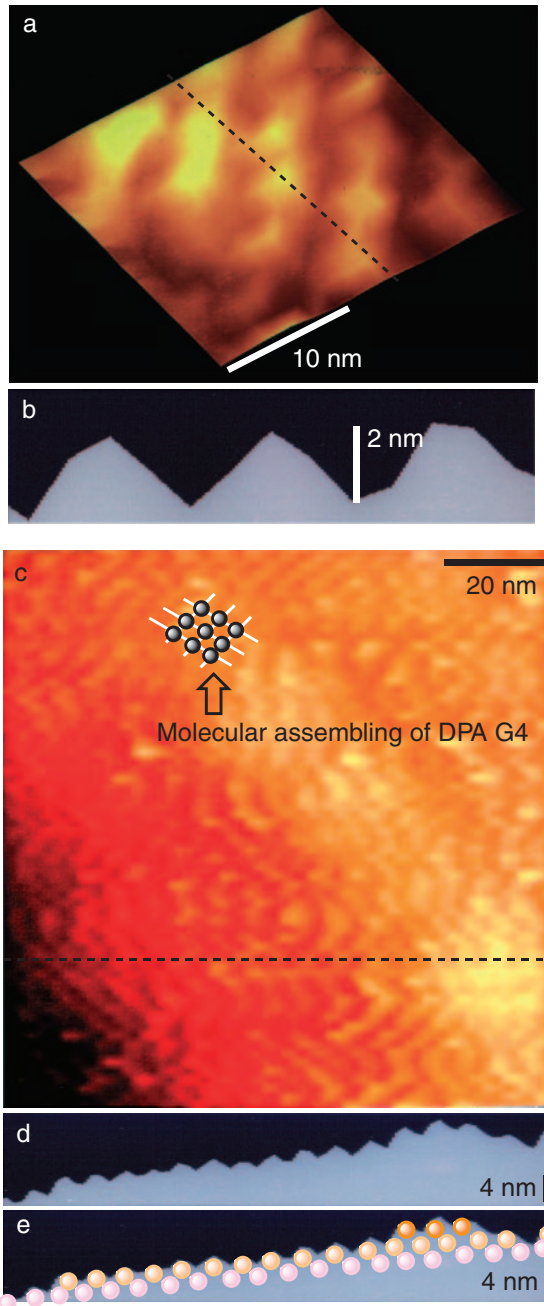

Fig. 6. (a) AFM pictures of DPA G4 (25 × 25 nm) and (b) a cross section at the dotted line of Fig. 6a. (c) AFM pictures of DPA G4 (125 × 125 nm) and (d) a cross section at the dotted line of Fig. 5c. (e) Schematic representation of the multilayered assembling of DPA G4.

ation, the molecular structure of DPA became three-dimensionally expanded due to the steric hindrance among the branches. As a result, a DPA G4 molecule was postulated to have a sphere-like structure (2.5 × 2.9 × 2.3 nm) with four horns in the solid state.

1.3 Molecular Assembling (TEM, AFM, and π–A Measurements). DPA G4 molecules were confirmed by TEM to have a round shape with a 2.3 ± 0.3-nm diameter (Fig. 5). We noticed that the 2.3-nm diameter is much smaller than those of a similar generation of reported dendrimers consisting of a

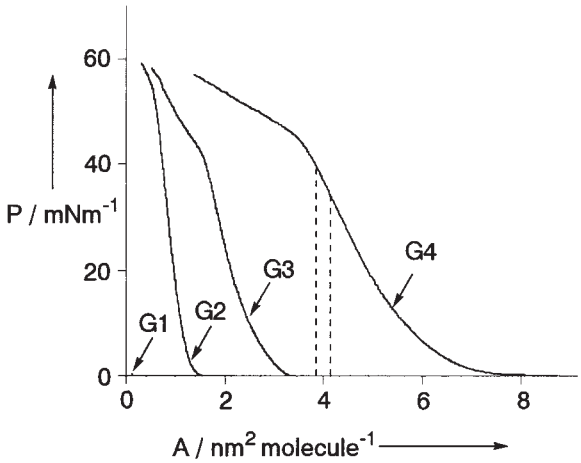

Fig. 7. π–A measurement of DPAs G1–4.

single bond backbone such as PAMAM. In the dendrimers having a single bond backbone, the diameter observed by TEM is much longer than expected, because the flexible backbones of the dendrimers cause the deformation of the molecule on a plate.[13] In other words, the small diameter of a DPA G4 molecule shows a three-dimensionally expanded structure without deformation on a plate. However, TEM pictures give little information as to the height. Therefore, in order to reveal the height of DPA G4 on a plate, AFM measurements were performed in the non-contact mode. DPA G4 molecules are revealed by AFM to be regularly assembled in a multi-layered packing structure on a graphite plate by casting (Figs. 6a–c). Though the resolution is close to the limit in the tapping mode, a lattice pattern was observed in the picture and the cross section clearly shows alignment of the spherical molecules in a multilayer. The height of the DPA G4 molecule was estimated from the cross section to be at least 2.0 ± 0.1 nm (Figs. 6d,e). The observed height will be smaller than the actual height of the dendrimer due to overlapping with the under layer. Therefore, these results revealed that the DPA G4 molecules have a sphere-like structure with about a 2.3-nm diameter, which almost agreed with that obtained by molecular modeling. Conformational rigidity of the π-conjugated backbone in DPA G4 enables the regular polymer-assembling on a plate without deformation of the molecule.

In π–A measurement, the size of DPA G4 was also estimated based on the occupied area of the molecule in a monolayer on water. The π–A isotherms of DPA G2–4 showed a transition behavior on pure water (Fig. 7). The DPA G4 curve rose with the limiting area of 3.8–4.2 nm^2. The diameter of a DPA G4 molecule was calculated from the area to be 2.2–2.3 nm, which agrees with that determined by the TEM result.

1.4 Molecular Conformation (GPC Analysis and NMR). The polymer morphology is also determined by gel permeation chromatograph (GPC) analysis,[14] because the linear and rigid polymers have shorter elution times than those expected from the molecular weight, while sphere-like polymers such as the dendrimers have longer ones. The M_n values of DPAs calculated using a polystyrene standard in GPC (M_n of DPA G1–4: 300, 1000, 2400, and 3800, respectively) were smaller than those determined by TOF-MS (M_n of DPA G1–4: 436, 1153, 2587, and 5451, respectively). The difference between the GPC and TOF-

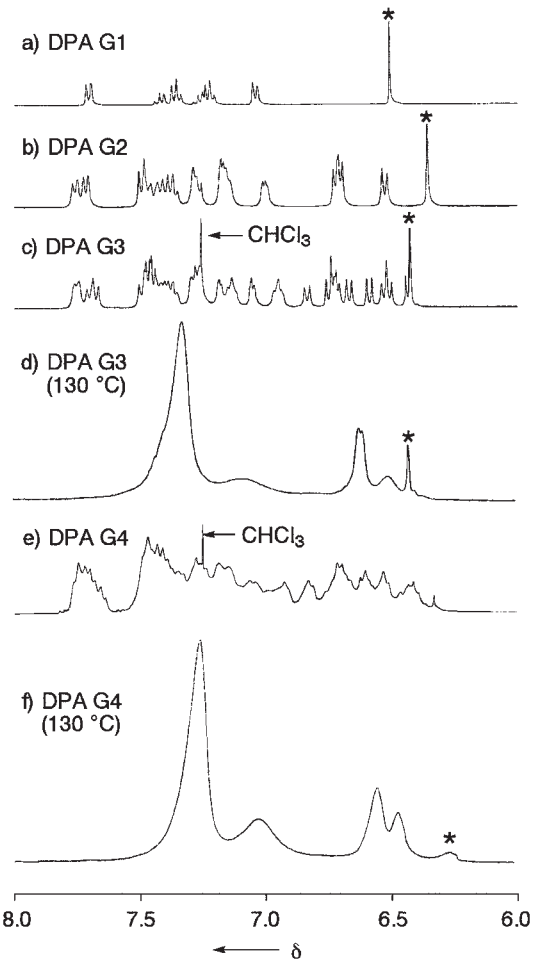

Fig. 8. ^{1}H NMR spectra of (a–c) DPAs G1–3 in $CDCl_3$ at 30 °C, (d) DPA G3 in DMSO-d_6 at 130 °C, (e) DPA G4 in $CDCl_3$ at 30 °C, and (f) DPA G4 in DMSO-d_6 at 130 °C. The marked peaks (*) are attributed to the four protons of the phenyl ring in the core of the DPAs.

MS results was especially significant in DPA G4, which shows that DPA G4 molecules are close to a compact sphere structure in solution as well as in the crystal.

In the ^{1}H NMR spectra of DPA G1–3, a singlet peak attributed to the four protons of the core phenyl ring was observed at 6.6–6.3 ppm; this supports the symmetrical structure of the DPAs (Figs. 8a–c). On the other hand, a singlet peak was not observed in the spectrum of DPA G4, because the conformation of the core imines is fixed by the bulky dendrons (Figs. 8d and 9). Therefore, a broad peak attributed to the four protons of the core appeared at 6.26 ppm in the spectrum of DPA G4 at high temperature (Fig. 8f). The appearance of this peak is based on the slight conformational exchange of the core imines in DPA G4, which was also supported by the comparison with the sharp peak in the core of DPA G3 at 130 °C (Fig. 8e).

1.5 Stepwise Radial Complexation with $SnCl_2$. DPA G1–4 have 2, 6, 14, and 30 imines, respectively, which coordinate strongly to various metal ions such as Sn, Ag, Eu, and Tb. DPA G4 should trap 30 equivalents of $SnCl_2$, because $SnCl_2$ has a coordinating site.[15] A color change from yellow to orange due to the complexation was observed during addition of $SnCl_2$

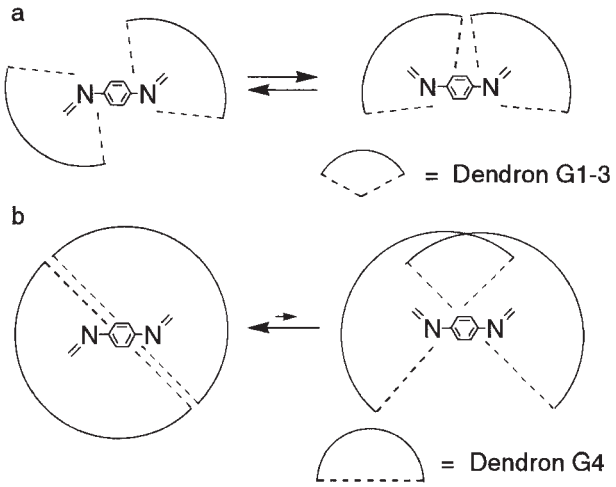

Fig. 9. Schematic representation of (a) conformational exchange at the core of DPA G1–3 and (b) fixed conformation at the core of DPA G4 by the bulky dendrons G4.

to a dichloromethane/acetonitrile solution of DPA G4. Using UV–vis spectroscopy to monitor the titration until 30 equivalents of $SnCl_2$ have been added, one could observe four time changes in the position of the isosbestic point, indicating that the complexation proceeds not randomly, but stepwise (Fig. 10). The spectral changes were finished within 10 minutes after addition of $SnCl_2$. An isosbestic point appears when a compound is quantitatively transformed into another by complexation, so the four shifts in the isosbestic point suggest that four different complexes are successively formed on $SnCl_2$ addition.

The spectra of DPA G4 gradually changed, with an isosbestic point at 375 nm up to the addition of two equivalents of $SnCl_2$. The isosbestic point then shifted on further addition of $SnCl_2$ and appeared at 364 nm between three and six equivalents. During the addition of between seven and 14 equivalents of $SnCl_2$, an isosbestic point appeared at 360 nm; this moved to 355 nm on adding between 15 and 30 equivalents. Overall, the isosbestic point shifted about 20 nm from 375 to 355 nm, and the number of added equivalents of $SnCl_2$ required to induce a shift was in agreement with the number of imine sites present in the different shells of DPA G4. From a kinetic standpoint, complexation of the terminal imines of the dendrimer is expected to occur first. However, the titration results suggest that, on the timescale of our observations, the process is thermodynamically controlled and proceeds in a stepwise fashion from the core imines to the terminal imines of DPA G4.

Similar stepwise complexation was also observed with DPA G2 and G3 (Fig. 11). For DPA G2, two isosbestic points appeared at 344 and 355 nm on adding 0–2 and 3–6 equivalents of $SnCl_2$, respectively. For DPA G3, three isosbestic points appeared at 367, 360, and 355 nm on adding between 0–2, 3–6, and 7–14 equivalents of $SnCl_2$, respectively. Again, the equivalents of $SnCl_2$ added before a shift in isosbestic point is observed agree with the number of imine sites present in the different shells of the two dendrimers. These results further supported the idea that metal ions are incorporated in a stepwise fashion, filling first the shell close to the dendrimer core and then progressively the more peripheral shells.

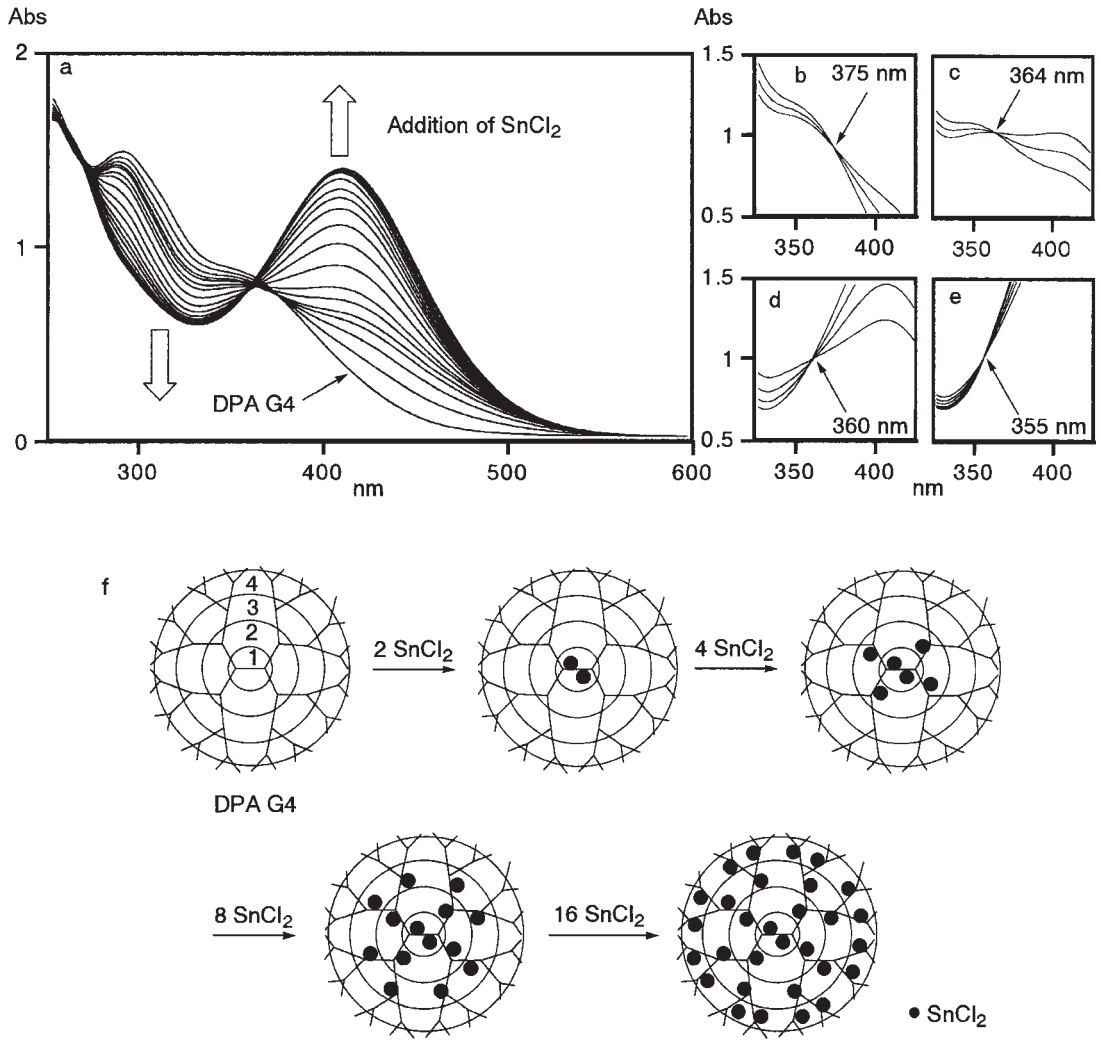

Fig. 10. UV–vis spectra of DPA G4 (5×10^{-6} M) complexed with (a) 0–30, (b) 0–2, (c) 3–6, (d) 7–14, and (e) 15–30 equiv. of $SnCl_2$ (solv. 1:1 dichloromethane:acetonitrile), and (f) schematic representation of stepwise radial complexation of DPA G4 with $SnCl_2$.

1.6 Shell Selective Reduction (SSR) of Imines in DPAs. In order to confirm the stepwise complexation except for UV–vis spectral measurements, we exploited a novel shell-selective reduction (SSR) method for imines in DPAs based on the reduction of imines to amines accelerated by complexation with $SnCl_2$. Because only the imine groups that are complexed with $SnCl_2$ in DPAs are reduced during the reduction of the complexes, the positions of $SnCl_2$ molecules in the DPA complexes are exactly determined by identification of the product after reduction of the complex. During the reduction of DPA G1 complexed with two equivalents of $SnCl_2$ in the presence of $NaBH_4$, the two imine sites were quickly and quantitatively reduced to amines. Interestingly, during the reduction of DPA G2 complexed with two equivalents of $SnCl_2$, only two imines at the 1st shell were selectively reduced to amines (DPA-red G2, a 90% NMR yield, Fig. 12). This result clearly supports the idea that two equivalents of $SnCl_2$ are complexed with the two imines of the 1st shell in DPA G2 (Fig. 12a). DPA-red G2 was assigned by NMR and MS measurements. In the ^{1}H NMR spectrum of DPA G2, two pairs of doublet peaks (1*trans*, 1*cis*) attributed to the 1st shell of the *C*-connected phenyl rings appear, based on the *cis*- or *trans*-conformation for the core phenyl ring (Fig. 12b).[7] On the other hand, in the spectrum of DPA-red G2, only one pair of doublet peaks (1) attributed to the *C*-connected phenyl rings appears, due to the disappearance of the regio-conformation, and one pair of doublet peaks (*x*, *y*) attributed to the reduced imines appears around 5.2 ppm (Fig. 12c). The TOF-MS spectrum is also useful in determining the positions of the amine groups in DPA-red G2, because the fragment peak based on easy cleavage of the C–N single bond appears in the spectrum. In the spectrum of DPA-red G2, the fragment peak at 524.2 shows the cleavage of the C–N single bond at the first shell (Fig. 11d).

The SSR method was also performed with DPA G4. During the reduction of DPA G4 complexed with two equivalents of $SnCl_2$, the imines at the first shell were selectively reduced to amines. The TOF-MS spectrum of the reduced product, DPA-red G4, clearly supported the claim that the amine groups are at the first shell; a fragment peak at 2674.9 appears based on the cleavage of the C–N single bond at the first shell (Fig. 13). In the ^{1}H NMR spectrum of DPA G4, a singlet peak attributed to the core protons did not appear, due to the fixed conformation of the core by the bulky G4 dendrons (Fig. 9), but a singlet peak attributed to the core protons appeared in

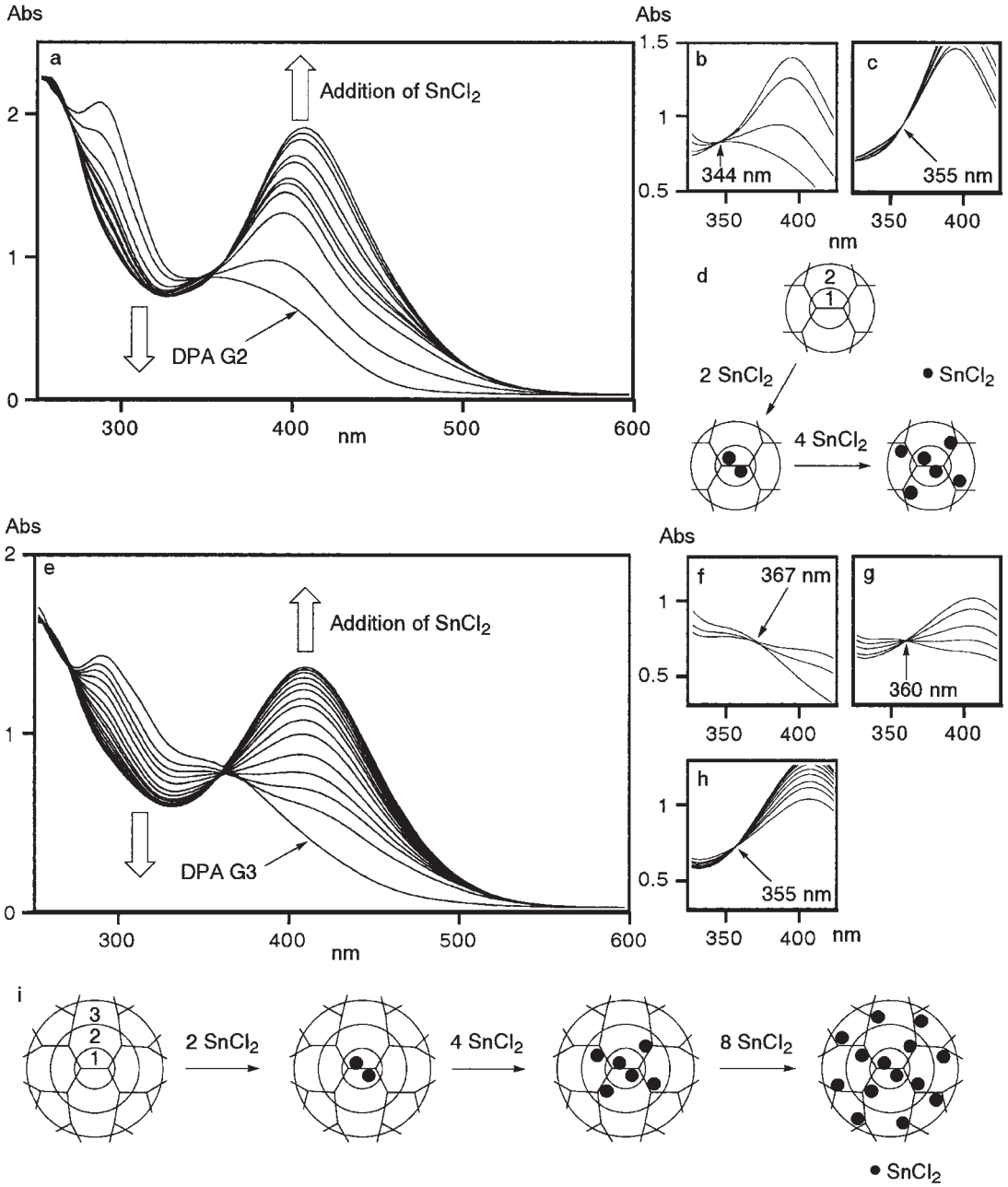

Fig. 11. UV–vis spectra of DPA G2 (3×10^{-5} M) complexed with (a) 0–6, (b) 0–2, and (c) 3–6 equiv. of $SnCl_2$ (solv. 1:1 dichloromethane:acetonitrile), and (d) schematic representation of stepwise radial complexation of DPA G2 with $SnCl_2$. UV–vis spectra of DPA G3 (1×10^{-5} M) complexed with (e) 0–14, (f) 0–2, (g) 3–6, and (h) 7–14 equiv. of $SnCl_2$ (solv. 1:1 dichloromethane:acetonitrile), and (i) schematic representation of stepwise radial complexation of DPA G3 with $SnCl_2$.

the spectrum of DPA-red G4. This result also supports the idea that two molecules of $SnCl_2$ are complexed with the two imines in the first shell of a DPA G4 molecule.

1.7 Stepwise Complexation Behavior in NMR Measurement. The stepwise complexation in DPAs with $SnCl_2$ was also supported by the NMR titration results (Fig. 14). In the ^1H spectrum of DPA G2, a singlet peak attributed to the four protons of the core phenyl ring was shifted to a lower magnetic field on addition of $SnCl_2$, due to the coordination to the imine nitrogen. The shift was large up to a two-equivalent addition of $SnCl_2$, and the shift became smaller with the further addition of $SnCl_2$. This spectral change supports the idea that the complexation of $SnCl_2$ first occurs at the core imines in DPA G2.

1.8 The Expanded Molecular Size of DPA G4 due to Trapping $SnCl_2$ Molecules. Based on the strong coordination ability of the imine groups, DPA G4 incorporates 30 equivalents of $SnCl_2$. The quantitative complexation of DPAs with 30 equivalents of $SnCl_2$ was supported by atomic absorption spectroscopy (AAS). The atomic absorption spectrum of DPA G4 fully complexed with $SnCl_2$ shows that at least 29 molecules of $SnCl_2$ are trapped in a DPA G4 molecule (Sn content in DPA G4 complexed with 30 equivalents of $SnCl_2$; calcd, 31.96%; found, 31.0%). The coordination of imine groups to $SnCl_2$ in the complexes of DPAs was confirmed by the IR spec-

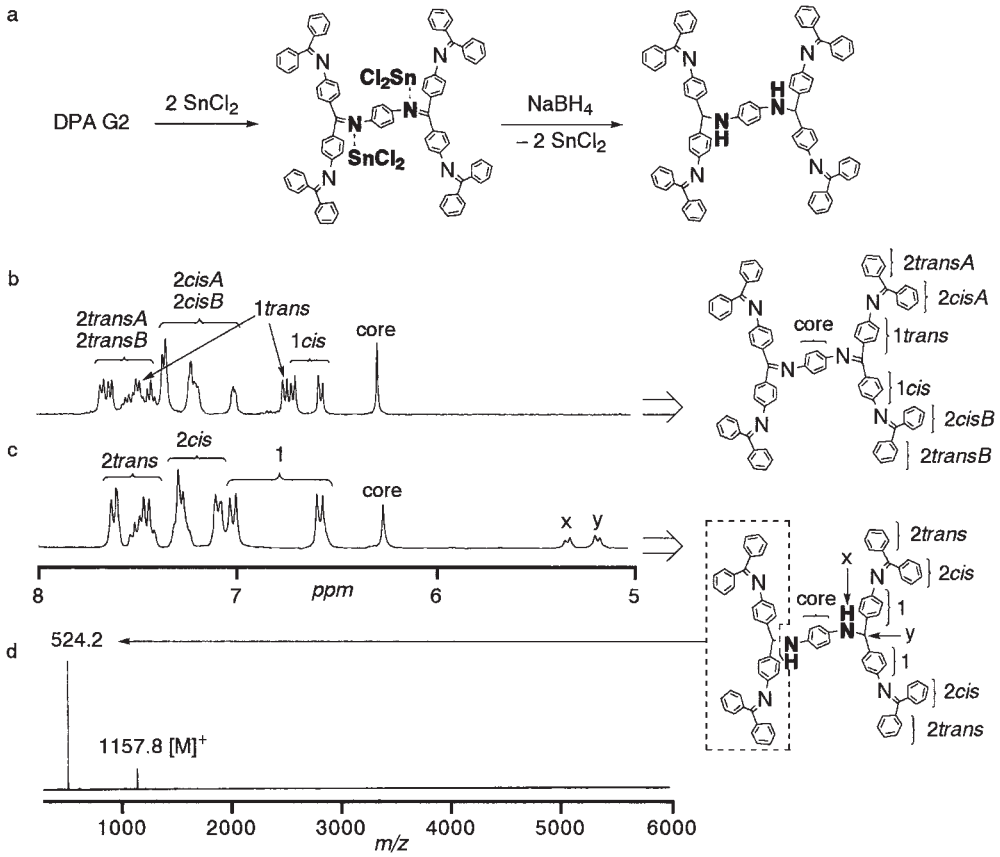

Fig. 12. (a) Shell-selective reduction of imines in DPA G2 complexed with two equivalents of $SnCl_2$. The ^1H NMR spectra (400 MHz, DMSO-d_6) of (b) DPA G2 and (c) the main product obtained by reduction of the complex (DPA-red G2). (d) MALDI-TOF-MS spectrum of DPA-red G2.

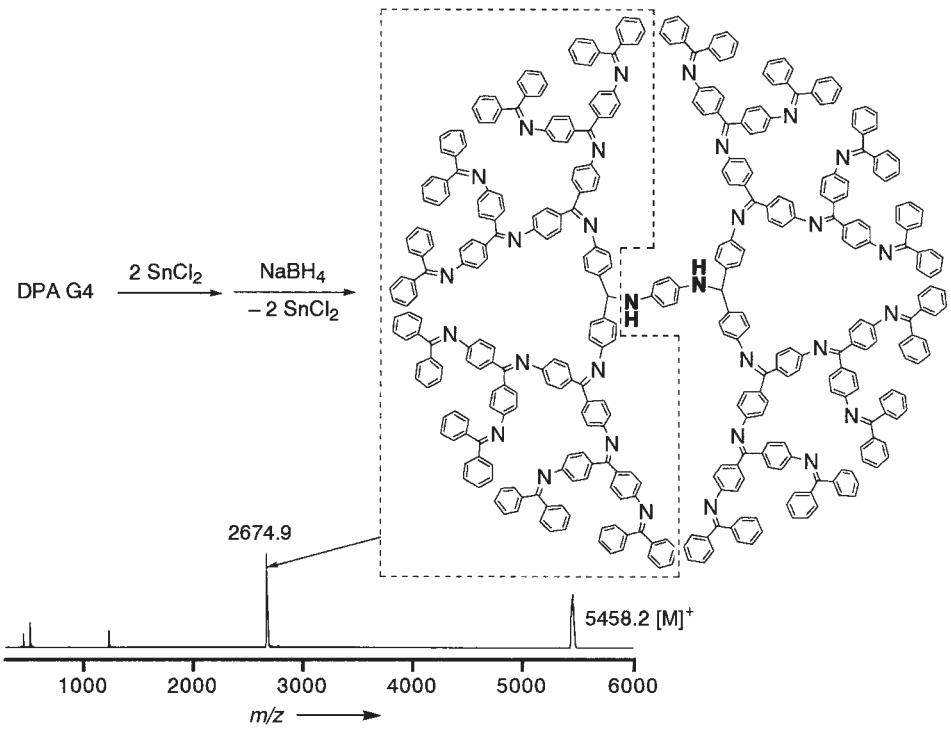

Fig. 13. MALDI-TOF-MS spectrum of DPA-red G4.

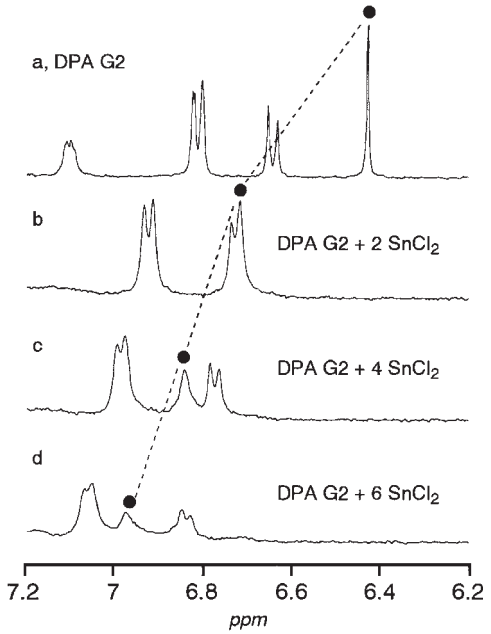

Fig. 14. The ^{1}H NMR spectra (400 MHz, dichloromethane-d_2/acetonitrile-d_3 = 1:1, 7.2–6.2 ppm only) of (a) DPA G2 and the complex with (b) two, (c) four, and (d) six equiv. of $SnCl_2$. The marked peaks (*) are attributed to the four protons of the core phenyl group in the DPA G2.

tral measurement. The absorption attributed to the stretching vibration of the imine bond (1617 cm^{-1}) of DPA G4 was shifted to 1624 cm^{-1} by the complexation; a similar shift was observed in DPAs G1–3.

In addition, trapping $SnCl_2$ molecules causes the expansion of the molecular size of DPA G4. Molecular modeling of DPA G4 complexed with 30 equivalents of $SnCl_2$ was performed based on structural information on bond length, angles, and dihedral angles taken from the X-ray crystal structures of DPA G2 and the reported imines complexed with $SnCl_2$ (Fig. 15a). The result of the modeling shows that (1) a DPA G4 molecule can trap 30 equivalents of $SnCl_2$ by conformational changes in the branches, and (2) the size of the complex (2.8 × 2.9 × 3.0 nm) is larger than that for DPA G4 (2.3 × 2.5 × 2.9 nm). The expansion of the molecular size by the complexation was supported by TEM; the TEM image of DPA G4 complexed with 30 equivalents of $SnCl_2$ shows a round shape with a 2.7-nm diameter (Fig. 15b), which is larger than that for DPA G4 (2.3-nm).

The stepwise radial complexation was also supported using TEM. Organic polymers, in general, are inverted on RuO_4 vapor before the TEM measurement in order to enhance the contrast of the TEM images, but metal atoms such as tin appear as TEM images without (or after a very short time of) the inversion. Therefore, the assembling state of $SnCl_2$ inside DPAs is confirmed by the TEM images of the complex without (or after

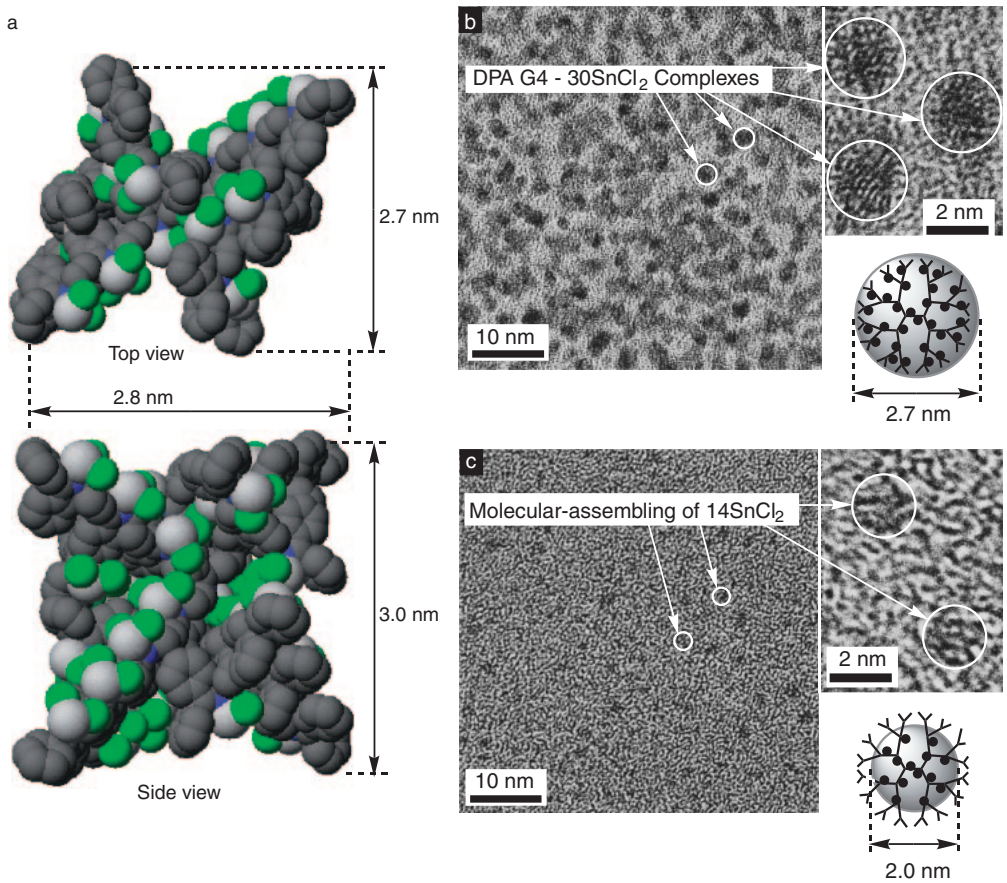

Fig. 15. (a) Molecular modeling of DPA G4 complexed with 30 equiv. of $SnCl_2$. TEM images of (b) DPA G4 complexed with 30 equiv. of $SnCl_2$, and (c) DPA G4 complexed with 14 equiv. of $SnCl_2$, which was inverted on RuO_4 vapor for 1 min.

a very short time of) the inversion. In the TEM image of DPA G4 complexed with 14 equivalents of $SnCl_2$, [the sample was inverted on RuO_4 vapor for a very short time (within 1 min)], the assembly of $SnCl_2$ was observed as a round shape with a 2.0-nm diameter (Fig. 15c). The 2.0-nm diameter is smaller than that in DPA G4. This result directly supports the idea that 14 equivalents of $SnCl_2$ molecules are complexed with the imines not randomly but stepwise up to the 3rd shell of DPA G4. After the full inversion (more than 15 min), a DPA G4 molecule complexed with 14 equivalents of $SnCl_2$ was confirmed to be a round shape with a 2.5-nm diameter, which shows the whole size of the complex.

1.9 The Gradients in the Basicity of Imine Groups in DPAs. The gradients in the basicity of imine groups that the basicity of the core imines is higher than that of the more peripheral imines is considered to cause the stepwise complexation behavior in DPAs. The high basicity of the core imines was confirmed in the ^{13}C NMR spectra of DPAs as a high magnetic field shift of the peak attributed to the core imine carbon. The marked (*) peaks in the spectra of DPAs were attributed to the core imine carbon (Fig. 16), which were determined by the SSR method and the comparison of their spectra. In the spectra of DPA G2 and G3, the marked peaks are shifted by more than 1 ppm towards a high magnetic field, relative to the peaks attributed to an imine carbon at the periphery (Figs. 16a–c). These spectra show that the basicity of the core imines is enhanced by the electron-releasing effect of the more peripheral imines.

1.10 Control of Stepwise Radial Complexation (DPA-F, DPA-Cl, and DPA-Me). Introduction of electron-withdrawing or -releasing groups to the core of DPAs was revealed to change the gradient of basicity among the shells of the DPAs. We synthesized novel DPAs having a 2,3,5,6-tetrafluoro-, 2,5-dichloro-, 2,5-dimethyl-substituted phenyl ring at the core (DPA-F G1–3, DPA-Cl G1–3, and DPA-Me G1–2) via dehydration of the DPA dendrons with tetrafluoro-, 2,5-dichloro-, and 2,5-dimethyl-*p*-phenylenediamine, respectively (Scheme 2). Introduction of fluorine to the core in DPAs strongly reduced the basicity of the core imines; this was confirmed by both the decrease of the complexation constant determined using UV–vis spectral titration and a low magnetic field shift of the peak attributed to the imine carbons in ^{13}C NMR spectrum. The complexation constant of an imine in DPA-F G1 is $\log K = 2.9$ (DPA G1: $\log K = 5.0$), and a peak attributed to the core imine in DPA-F G1 appears at 175.75 ppm in ^{13}C NMR spectrum (DPA G1: 167.97 ppm) (Figs. 16a and 16d). In the UV–vis spectral measurement of DPA-F G2, two isosbestic points appeared at 283 and 286 nm upon adding 0–4 and 5–6 equivalents of $SnCl_2$, respectively (Figs. 17a–c). This result shows that the imines present in the 2nd shell were completed first, then those present in the 1st shell, whose basicity was lowered by the electron-withdrawing tetrafluorophenyl group (Fig. 17d). On adding $SnCl_2$ to DPA-F G3, three isosbestic points appeared at 356, 366, and 368 nm upon adding 0–4, 5–12, and 13–14 equivalents of $SnCl_2$, respectively (Figs. 17e–h). That is, the imines present in the 2nd shell were completed first, then those present in the 3rd shell, and finally those present in the 1st shell (Fig. 17i). The shell order of the stepwise complexation in DPAs was controlled by the change of the gradients of basicity among the shells.

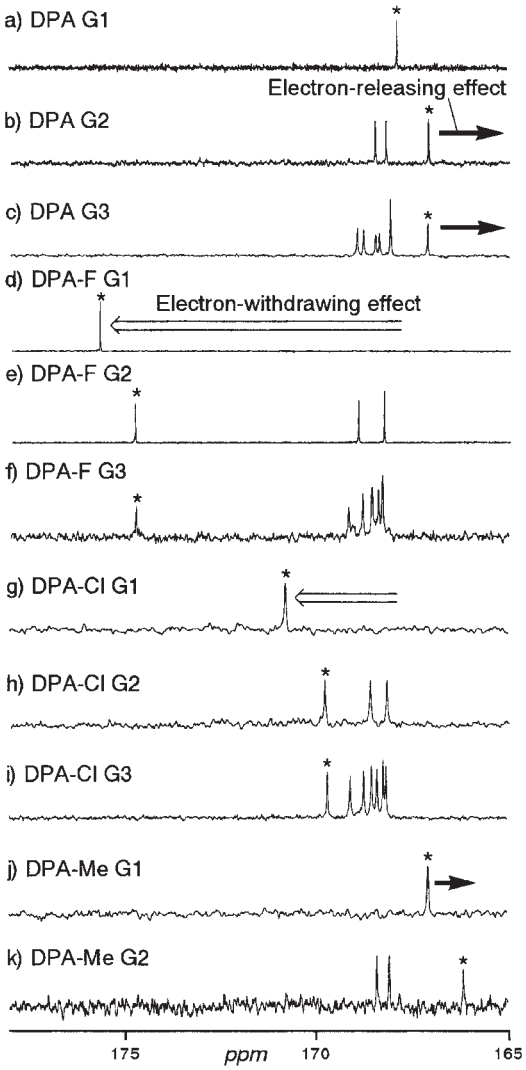

Fig. 16. The ^{13}C NMR spectra (100 MHz, TMS, ppm, only 165–180 ppm) of (a) DPA G1, (b) DPA G2, (c) DPA G3, (d) DPA-F G1, (e) DPA-F G2, (f) DPA-F G3, (g) DPA-Cl G1, (h) DPA-Cl G2, (i) DPA-Cl G3, (j) DPA-Me G1, and (k) DPA-Me G2. The marked peaks (*) are attributed to core imine carbons.

The SSR method in DPA-F G2 clearly supported the "reversed" pattern of complexation (Fig. 18). The reduction of DPA-F G2 complexed with four equivalents of $SnCl_2$ gave DPA-F G2 having four amines at the 2nd shell (DPA-F-red G2, an 80% NMR yield). This result shows that four equivalents of $SnCl_2$ are complexed with the four imines of the 2nd shell in DPA-F G2 (Fig. 18a). In the ^1H NMR spectrum of DPA-F G2, four sets of peaks (2*trans*A, 2*cis*A, 2*trans*B, 2*cis*B) attributed to the 2nd shell of the *C*-connected phenyl rings appear based on the *trans*,*trans*-, *trans*,*cis*-, *cis*,*trans*- and *cis*,*cis*-conformation for the core phenyl ring and the 1st shell of the *C*-connected phenyl ring, respectively (Fig. 18b). On the other hand, in the spectrum of the product, DPA-F-red G2, peaks (2) attributed to the 2nd shell of *C*-connected phenyl rings became simple due to the disappearance of the regio-conformation for the 1st shell of the *C*-connected phenyl ring, and two

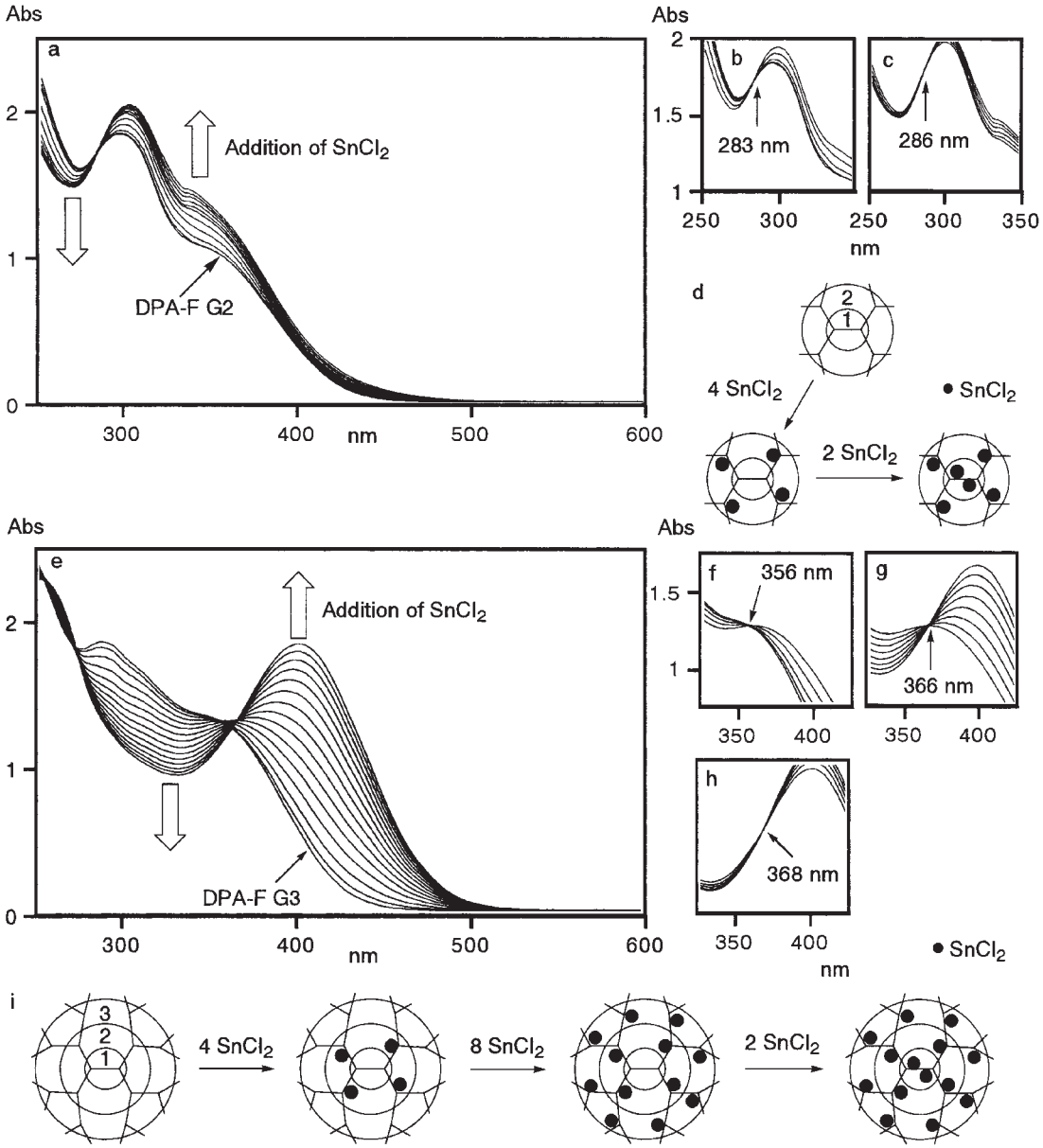

Fig. 17. UV–vis spectra of (a) DPA-F G1 (6×10^{-5} M) complexed with $SnCl_2$, and DPA-F G2 (3×10^{-5} M) complexed with (b) 0–8, (c) 0–4, (d) 5–8 equiv. of $SnCl_2$, and DPA-F G3 (1×10^{-5} M) complexed with (e) 0–18, (f) 0–4, (g) 5–12, (h) 13–18 equiv. of $SnCl_2$ (solv. 1:1 dichloromethane:acetonitrile). Schematic representation of stepwise complexation of (a) DPA-F G2 and (b) G3 with $SnCl_2$.

pairs of doublet peaks (xA yA, xB, yB) attributed to the reduced imines appears between 4.2–5.6 ppm due to the *cis*- or *trans*-conformation for the core phenyl ring (Fig. 18c). Two peaks at 169.03 and 168.36 ppm in the ^{13}C NMR spectrum of DPA-F G2 (Fig. 16e) disappeared in the spectrum of DPA-F-red G2, which shows that their peaks should be attributed to the terminal imines in DPA-F G2. The positions of amines in DPA-F-red G2 are also confirmed by the TOF-MS spectra. In the TOF-MS spectrum, the fragment peak at 1065.5 shows the cleavage of the C–N single bond at the 2nd shell (Fig. 18d).

Introduction of chlorine to the core of DPAs also reduced the basicity of the core imines. The complexation constant of an imine in DPA-Cl G1 ($\log K = 4.3$) was between those of DPA-F G1 and DPA G1. In the ^{13}C NMR spectrum, a peak attributed to the core imine in DPA-Cl G1 appears at 170.85 ppm, which also exists between those of DPA G1 and DPA-F G1 (Fig. 16g). In the UV–vis spectral measurement of DPA-Cl G2, two isosbestic points appeared at 315 and 294 nm upon adding 0–4 and 5–6 equivalents of $SnCl_2$, respectively. This result shows the "reverse" complexation pattern, which is the same as that in DPA-F G2. When adding $SnCl_2$ to DPA-Cl G3, three isosbestic points appeared at 353, 365, and 373 nm upon adding 0–4, 5–12, and 13–14 equivalents of $SnCl_2$, respectively. This result shows that the complexation pattern is in the order of the 2nd, 3rd, and 1st shells. On the other hand, introduction of methyl groups to the core enhanced the basicity of the core imines. The complexation constant of an imine in DPA-Me G1 ($\log K = 5.4$) was higher than that in DPA G1.

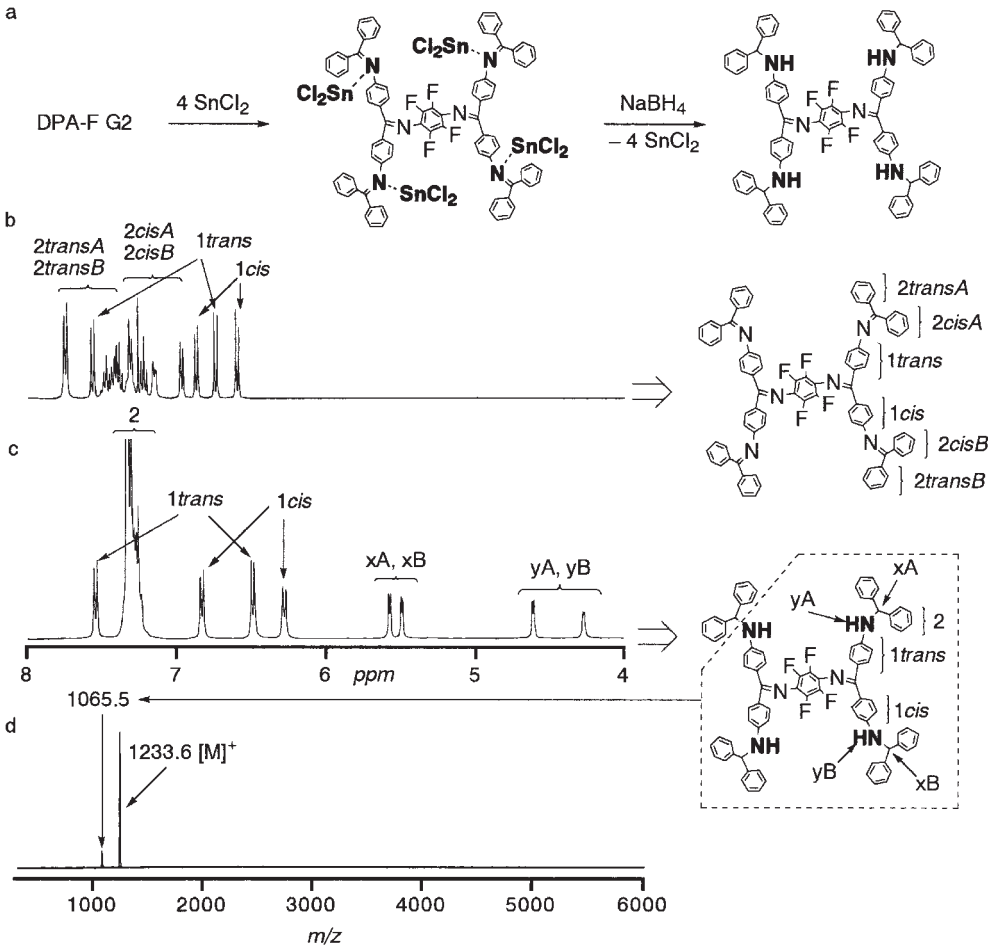

Fig. 18. (a) Reduction of imines in DPA-F G2 complexed with four equiv. of $SnCl_2$. The ^1H NMR spectra (400 MHz, DMSO-d_6) of (b) DPA-F G2 and of (c) the main product obtained by reduction of the complex. (d) MALDI-TOF-MS spectrum of DPA-F-red G2.

The higher basicity of imines in DPA-Me G1 than that in DPA G1 is also confirmed by ^{13}C NMR measurements; a peak attributed to the core imine in DPA-Me G1 appears at 167.10 ppm, which is at a higher magnetic field than that of DPA G1 (Fig. 16j). On addition of $SnCl_2$ to DPA-Me G2, two isosbestic points appeared at 327 and 345 nm upon adding 0–2 and 3–6 equivalents of $SnCl_2$, respectively. This behavior is similar to that of DPA G2 and shows the "normal" stepwise complexation pattern.

These complexation patterns in DPA derivatives are supported by the chemical shifts of the peaks attributed to the imine carbons in the ^{13}C NMR spectra. In the spectra of DPA-F and DPA-Cl, whose complexation patterns are in the order of the 2nd, 3rd, and 1st shells, the chemical shifts attributed to a core imine carbon is at a lower magnetic field than those of a branch imine carbon (around 168 ppm) (Figs. 16e, 16f, 16h, and 16i). On the other hand, in the spectra of DPA and DPA-Me, whose complexation pattern is in the order of the 1st, 2nd, and 3rd shells, the chemical shifts attributed to the core imine carbons are at a higher magnetic field (Figs. 16b, 16c, and 16k).

2. Cyclic Polyphenylazomethines

2.1 Selective Synthesis of Cyclic Phenylazomethine Trimers. Similarly to DPA, cyclic polyphenylazomethines are also expected as novel polymeric ligands with a single molecular weight and a single structure. Cyclic aromatic oligomers were synthesized under hyper-diluted conditions in order to promote the intramolecular reaction,[16] but there have been few reports about the highly selective preparation of a discrete cyclic aromatic in a one-step reaction. PPAs have been synthesized during dehydration of aldehydes or methylketones with amines. However, cyclic oligomers are not obtained at all during the polymerization, because the *E*-conformational imine is thermodynamically more stable than the *Z*-one. In other words, control of the *E*/*Z* conformation is very important for the synthesis of cyclic polyphenylazomethines (CPA). No cyclic oligomers were formed during the dehydration of 4′-aminoacetophenone in the presence of $TiCl_4$, but a novel cyclic phenylazomethine trimer (CPA3-ab, designated as CPAX-Y where X and Y are the degree of polymerization and whether the polymerization was AB- or AABB-type, respectively) was obtained in a 20% yield under non-dilute conditions ([monomer] = 0.1 M) during the dehydration of 4-aminobenzophenone (Scheme 3). The yield is considerably higher than those of previously reported cyclizations such as carbonate and thiophenylene compounds. PPA was obtained as a side-product in this reaction. In the presence of $TiCl_4$, the yield of CPA3-ab was enhanced by the induction of the bulky substituents at the α-position of the substrate. The dehydration of 4-amino-4′-octylaminobenzophenone resulted in the formation of the corre-

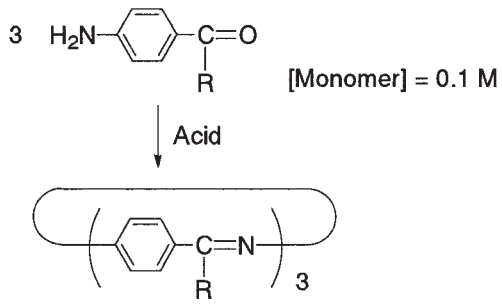

Cyclic phenylazomethine trimer (AB-type polymerization)

CPA3-ab

R	Yield, %	
	$TiCl_4$ (0.75 equiv.)[a]	PTS (0.05 equiv.)[b]
Me	0[c]	0[c]
Ph	20[c]	90
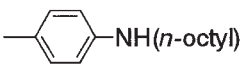 NH(*n*-octyl)	49	32
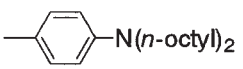 $N(n\text{-octyl})_2$	92	trace[d]

[a] Solv.: chlorobenzene, 125 °C, 15 h.
[b] Solv.: *p*-xylene, reflux, 16 h.
[c] The other products were the polymeric compounds.
[d] The other products were the oligomers up to pentamer.

Scheme 3. Synthesis of CPAs.

sponding cyclic trimer in a 49% yield. The dehydration of 4-amino-4′-dioctylaminobenzophenone gave the corresponding trimer in a 92% isolated yield. On the other hand, a different reaction behavior was observed in the presence of *p*-toluenesulfonic acid (PTS). The dehydration of 4′-aminoacetophenone by PTS gave the corresponding polymer similar to the dehydration by $TiCl_4$, but CPA-a was obtained in a 90% yield by the dehydration of 4-aminobenzophenone. Contrary to the case of $TiCl_4$, the induction of a bulky substituent produced a lower yield of CPA. The other products were confirmed by GPC to be the oligomers up to pentamer. The yields of CPAs are drastically influenced by the different reactivity between $TiCl_4$ and PTS, which was caused by their different coupling mechanisms. CPAs are formed through the intramolecular coupling of the linear trimer with the *Z*,*Z*-conformation. Because the dehydration using $TiCl_4$ is an irreversible reaction, the yield of CPAs is controlled by the ratio of the *E*/*Z* isomers. The *Z* isomer of phenylazomethine trimer (OPA3, which is described later) is formed in about a 50% yield, as was confirmed by the NMR spectrum. Therefore, CPA3-ab having phenyl groups at the α-positions of the imines is theoretically formed in 25% (0.5^2) yield, which agrees with the experimental yield of 20%. The higher yields of CPA3-ab derivatives having aminophenyl groups are based on the preferential formation of the *Z* isomer due to steric effects of the bulky substituents. On the other hand, the dehydration using PTS is an equilibrium reaction, in which the ratio of the isomers is controlled by the thermodynamic process. Therefore, the exchange reaction between the *E*/*Z* isomers occurs through the transamination. In addition, the resulting CPA-a is insoluble in the reaction solvent, so the formation of CPA-a was accelerated in the equilibrium reaction. However, PTS was not useful for the dehydration of the monomers substituted with alkylaminophenyl groups at the α-position, because the π-conjugation of the monomers to the aminophenyl group at the α-position lowers the electrophilicity of the carbonyl carbon.

2.2 Dendrimer Synthesis Based on Selective Cyclization. A controlled cyclization based on the steric effect in the presence of $TiCl_4$ was applied for dendrimer synthesis.[17] The third generation of dendritic polyphenylazomethine having a cyclic phenylazomethine trimer as the core (DPA-C G3) was quantitatively obtained during the polymerization of a 4-aminobenzophenone derivative having a DPA G3 dendron as a bulky substituent, due to steric hindrance among the bulky dendrons (Fig. 19a). The DPA-C G3 obtained by filtration was pure enough without further purification by column chromatography. The TOF-MS spectrum (Fig. 19b) and GPC analysis (M_w/M_n = 1.03) show that DPA-C G3 is the sole compound with a single molecular weight. In the polymerization of 4-aminobenzophenone derivatives having DPA dendrons G1 and G2 (DPA-C dendrons G1 and G2), the corresponding dendrimers having a cyclic structure (DPA-C G1 and G2) were obtained in 42 and 70% yields, respectively. These results show that the increase in the generation of a dendron enhances the yield of the corresponding dendrimer due to the steric hindrance between the bulky dendrons.

The kinetic analysis using GPC in the polymerization of DPA-C G1 dendron revealed that the cyclotrimerization proceeds very rapidly and the formation of DPA-C G1 almost finishes within 10 min (Figs. 20a and 20c). Interestingly, the linear trimer was not detected at all by TOF-MS measurement even in the crude solution at the reaction time for 1 min (Fig. 20b). The absence of the linear trimer in the reaction mixture supports the belief that the cyclic trimers are formed mainly via the one-step synthesis rather than by a stepwise polymerization such as dimer $\Rightarrow$ linear trimer $\Rightarrow$ cyclic trimer.

2.3 Oligophenylazomethines. Oligophenylazomethines (OPAs) and the aniline-capped OPAs (OPA′s) were synthesized as comparative compounds of CPAs (Scheme 4). Using $TiCl_4$ as an additive agent, OPAs are synthesized via dehydration of 4-aminobenzophenone in the presence of benzophenone as a terminating molecule. Aniline-capped OPAs (OPA′s) are obtained in one-pot synthesis, but of course, OPA′s were also synthesized in high yields via stepwise dehydration of OPAs with aniline. These results support the belief that $TiCl_4$ is a useful dehydration agent to form additional imine bonds without hydration of the already-formed imine bonds, because the dehydration using $TiCl_4$ is an irreversible reaction, unlike PTS. The thermogravimetry results of the CPA3-ab, OPAs, OPA′s,

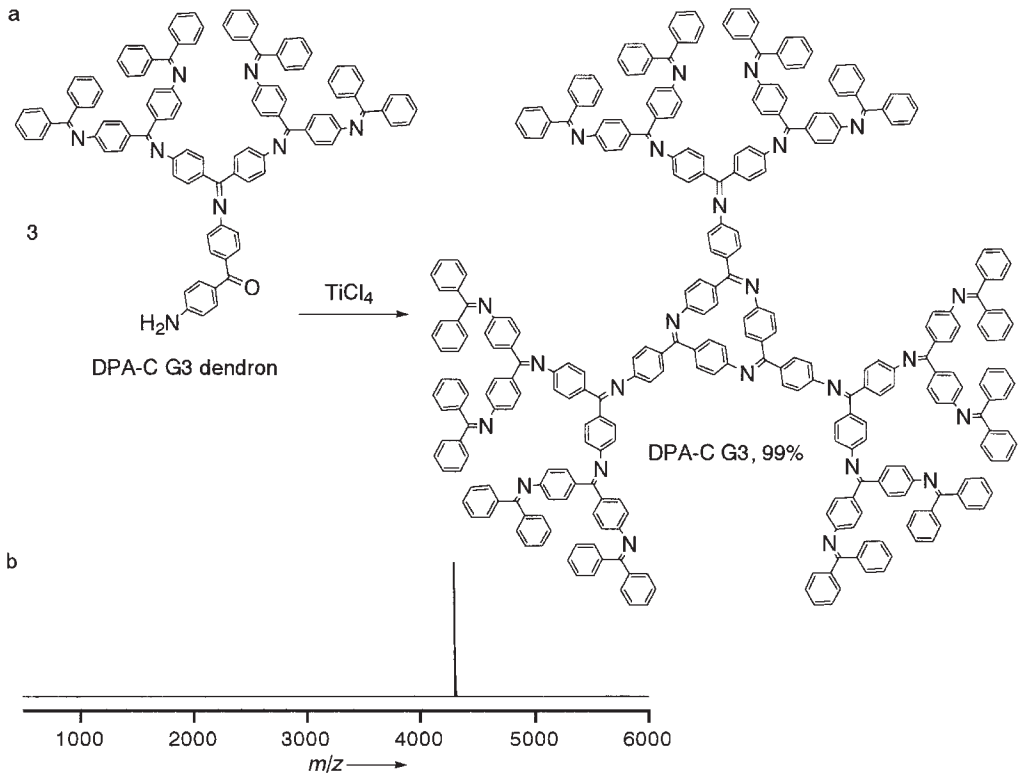

Fig. 19. (a) Highly selective synthesis of DPA-C G3 via controlled cyclization and (b) the TOF-MS spectrum of DPA-C G3 (4302 $[M + H]^+$).

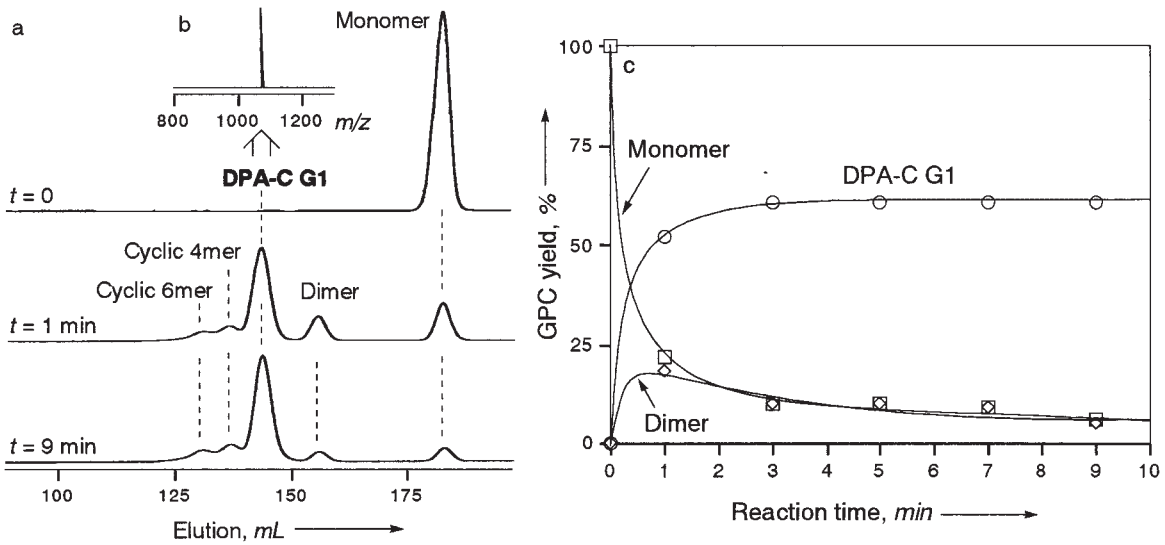

Fig. 20. Kinetic analysis using GPC in the polymerization of DPA-C G1 dendron. (a) GPC elution curves at the reaction time for 0, 1, and 9 min and (b) the TOF-MS spectrum of the trimer. (c) The relationship between the yields of DPA-C G1, the G1 dendron, and linear dimer and the reaction time.

and PPA show that each compound has a high thermostability due to the imine bond, which has a large bond energy (615 kJ/mol). The temperature for a 5% weight loss ($Td_{5\%}$) of OPA2, 3, 4, OPA2′, 3′, and PPA were determined to be 301, 368, 438, 326, 397, and 508, respectively, based on the thermogravimetric analysis. The $Td_{5\%}$ increased with an increase in the degree of polymerization and capping with aniline. This means that the carbonyl group at the end of the oligomer is more likely to initiate the thermal degradation. CPA3-ab shows a good $Td_{5\%}$ at 404 °C, which was close to that of OPA3′, due to the absence of an end group in the chain.

2.4 Spectroscopic Analysis of the CPA Structure. The ^{13}C NMR spectra show that OPA3 and OPA2′ have 2 isomers and OPA4 and OPA3′ have 4 isomers, respectively, based on the *E*/*Z* conformation of imines (Fig. 21). OPA3 has one carbonyl and two imines, but two peaks attributed to the carbonyl

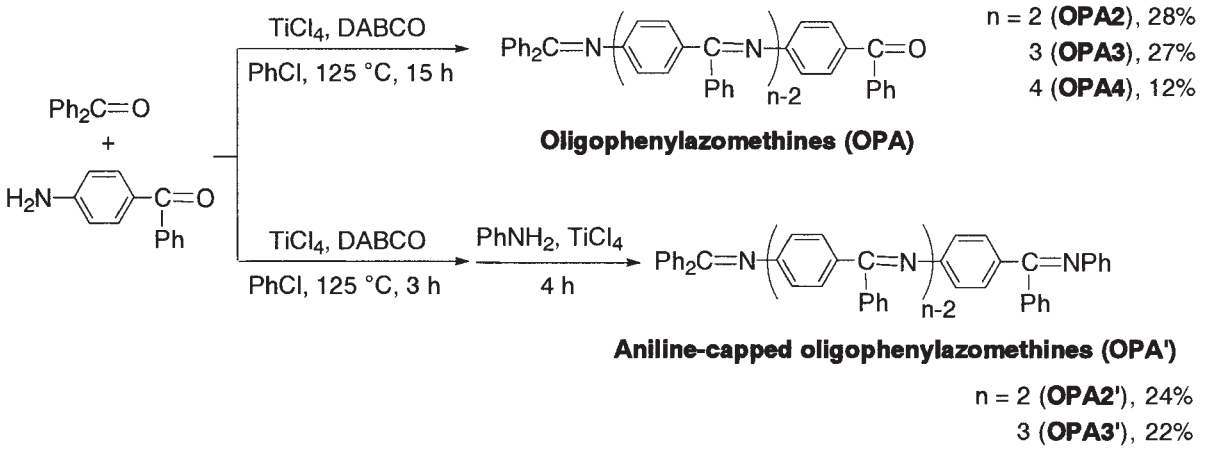

Scheme 4. Synthesis of OPAs.

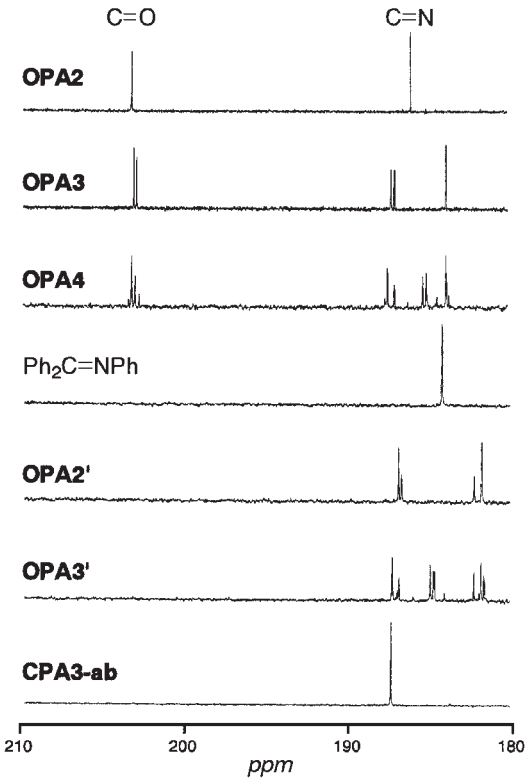

Fig. 21. The ^{13}C NMR spectra of OPAs, OPA′s, and CPA3-ab in CF_3COOD.

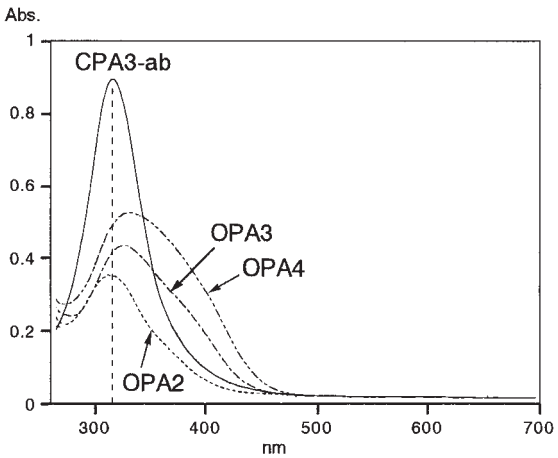

Fig. 22. The UV–vis spectra of a) OPA2, b) OPA3, c) OPA4, and d) CPA3-ab.

carbon at 203.04 and 202.85 ppm and four peaks attributed to the imine carbon at 187.20, 187.00, 183.83, and 183.80 ppm were observed in the spectrum (Fig. 21b). The formation ratio of the *E*/*Z* isomers in the OPA3 was estimated to be 1:1 based on the area ratio of the 2 peaks attributed to the carbonyl carbon. OPA4 has 1 carbonyl and 3 imines, but the spectrum shows four peaks attributed to the carbonyl carbon at 203.29, 203.11, 202.89, and 202.65 ppm and multiple peaks attributed to the imine carbon (Fig. 21c). On the basis of the integration ratio of each peak in the spectrum of OPA4 (the pulse sequence is NNE), the formation ratio of the four isomers was approximately estimated to be 9:6:3:1. Similar to OPA3 and OPA4, OPA2′ and OPA3′ showed multiple peaks corresponding to the isomeric structure. In OPA2′ with two imines, four peaks attributed to the imine carbon were observed at 168.96, 168.51, 168.21, and 167.86 ppm (Fig. 21e), and the spectrum of OPA3′ with three imines shows 12 peaks (Fig. 21f). OPA2 and Ph_2C=NPh had simple spectra due to the lack of *E*/*Z* isomers (Figs. 21a and d). On the other hand, only one peak attributed to the imine carbon in the spectrum of CPA3-ab shows the symmetrical structure having three *Z*-conformational imines (Fig. 21g).

E/*Z*-conformation of imines is also confirmed using UV–vis spectroscopy. The spectrum of CPA3-ab shows the shortest λ_{max} absorbed π–π^* transition of imine bonds at 318 nm (Fig. 22). On the other hand, in the spectra of OPAs, the absorption shifts to the longer wavelength according to the conformation. The *E* and *Z* isomers possess different electronic structures, of which the absorption band of the *E* isomer is shifted by about 20–50 nm to a longer wavelength than that of the *Z* isomer due to elongation of the π-conjugation. An MM2 calculation of CPA3-ab with only the *Z* conformation indicated that the three phenyl rings in the cyclic trimer do not have a coplanar structure. The structure of the *E* isomer also possesses a large distortion that builds up because of the large formation energy, as calculated by molecular modeling. Actually, the structure of CPA3-ab with three *Z*-conformational imine bonds

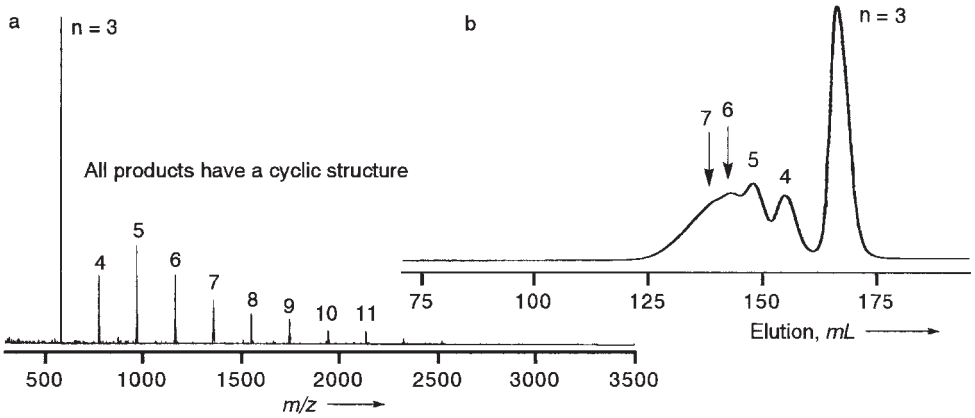

Fig. 23. (a) TOF-MS spectrum and (b) GPC analysis of the crude products during the polymerization of 4,4′-diaminobenzophenone in the presence of $TiCl_4(THF)_2$.

was confirmed by the X-ray crystal analysis described later.

2.5 Selective Cyclization in Hyperbranched Polymer Synthesis. In general, linear polymers are synthesized by the polymerization of AB-type monomers. On the other hand, the polymerization of multi-functional compounds such as AB_2-type monomers resulted in the formation of hyperbranched polymers. Similarly to the case of the linear polymerization, cyclization also proceeds to some extent during the hyperbranched polymerization,[18] but the isolation of a single cyclic oligomer in hyperbranched polymerization has not been reported to the best of our knowledge. It is because the yield of each cyclic oligomer is too low to isolate due to further polymerization between the cyclic oligomers with monomers in the reaction mixture. The cyclization is undesirable for hyperbranched polymer synthesis, but highly controlled cyclization has a possibility of providing novel functional materials or synthetic methods for hyperbranched polymers. From the viewpoint of functional materials, multi-functional cyclic oligomers are attractive building units for supramolecular systems, because they have a cavity for ion reception or molecular recognition and functional groups that can combine with other compounds by chemical and/or hydrogen bonds. We succeeded in the first controlled cyclization in hyperbranched polymer synthesis on the basis of a steric effect using a Lewis acid with bulky ligands. A multi-functional cyclic oligomer was isolated, and the structure including a cavity was determined by X-ray crystal analysis.

Though PTS and $TiCl_4$ are good dehydration agents for cyclization during AB-type polymerization of 4-aminobenzophenone derivatives, they were useless for the cyclic oligomerization in AB_2 type polymerization of 4,4′-diaminobenzophenone. The dehydration did not proceed in the presence of PTS, because the electrophilicity in the carbonyl carbon of the monomer is reduced by the π-conjugation expanded to the two aminophenyl groups. $TiCl_4$ is a powerful dehydration agent, but the dehydration led to the formation of only the insoluble phenylazomethine polymer due to the random polymerization. On the other hand, $TiCl_4(THF)_2$, which was formed by the rapid complexation of $TiCl_4$ with THF solvent, was revealed to work as a good dehydration agent for the cyclization, and the formation of only phenylazomethine oligomers with one cyclic structure were confirmed by the TOF-MS spectrum of the crude products. This TOF-MS spectrum is much different from those of general hyperbranched polymerization; only peaks attributed to oligomers having one cyclic structure appear in the spectrum (Fig. 23a). This result shows that the introduction of bulky THF groups in $TiCl_4$ strongly promotes the formation of the *Z*-conformational imine bonds by steric hindrance as shown in Fig. 24, and as a result, only oligomers having a cyclic structure were obtained. The GPC result of the crude products also supports the composition ratio of the respective oligomers shown by TOF-MS analysis (Fig. 23b).

The cyclic trimer having three amino groups as functional sites (CPA3-abb) was isolated and identified by X-ray crystal analysis (Fig. 25). The crystals were obtained by the slow vapor diffusion of methanol into a THF solution of CPA3-abb. As shown in Fig. 25, the imine nitrogen atoms have enough space outside the molecule to combine with $TiCl_4(THF)_2$, which led to the preferential formation of the *Z* conformational imine bond. The terminal amino group of CPA3-abb promotes the 2-dimensional dimerization by the formation of a hydrogen bond with the core imine of another molecule (the N–N distance: 3.20 Å).[6] The CPA3-abb has a cavity (19.6 $Å^2$) similar to that of [2.2.2]paracyclophane, which is a typical π-receptor for metal ions.

This cyclization method was also useful for cyclization during the linear polymerization of 4-aminobenzophenone. The yield (20%) of the cyclic trimer in the presence of $TiCl_4$ was enhanced to a 51% yield using $TiCl_4(THF)_2$. As a result, one way to control cyclization during the polymerization of both the AB_2 and AB type monomers was revealed to be using a Lewis acid with bulky ligands.

2.6 Phenylazomethine Macrocycles. In the presence of PTS, $TiCl_4$, or $TiCl_4(THF)_2$, cyclic phenylazomethine trimers are synthesized and isolated during the AB- and AB_2-type polycondensations. However, it is very difficult to isolate any macrocycles in the AABB-type polycondensation or the macrocycles except for the trimer in the AB- and AB_2-type polycondensations under the synthetic conditions. This is due to the formation of linear oligomers (in the case of AABB- and AB-type polycondensations) or the macrocycles randomly substituted by the monomer (in the case of AB_2-type polycondensation) that lowers the yields of the desired macrocycles and/or makes the isolation difficult. In other words, the total cyclization of the

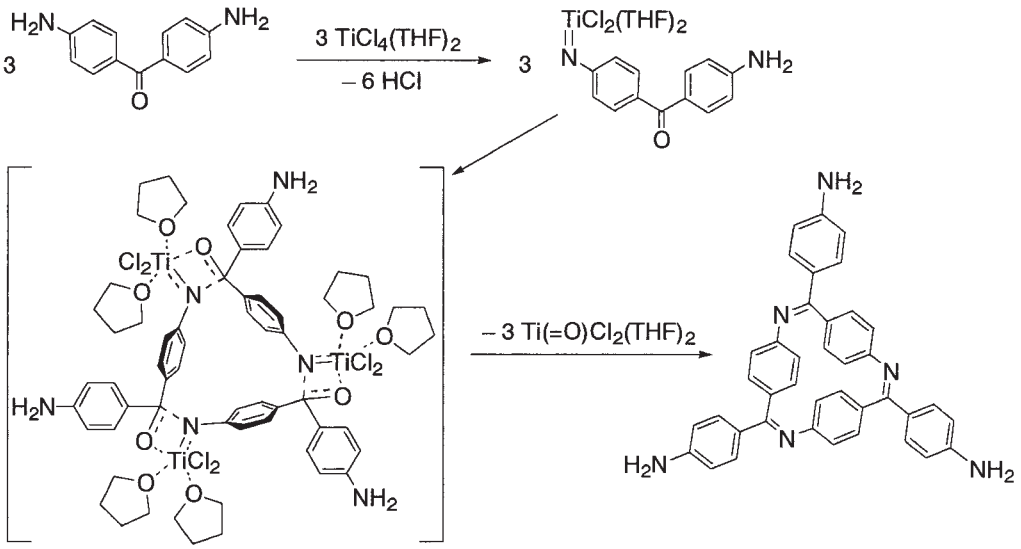

Fig. 24. Controlled cyclization in the presence of $TiCl_4(THF)_2$.

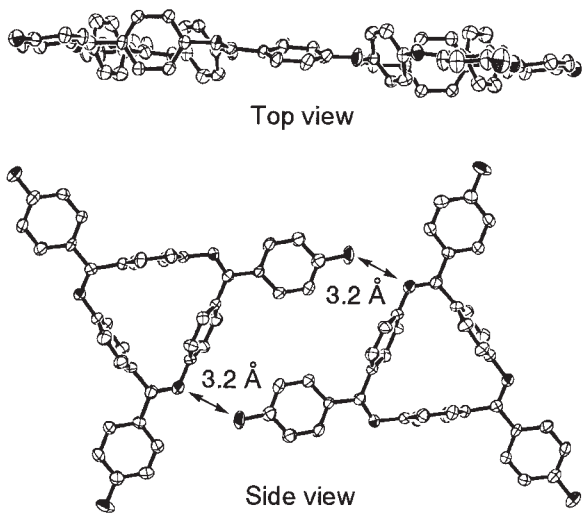

Fig. 25. ORTEP figure of CPA3-abb with 30% ellipsoid (hydrogen atoms are omitted).

linear oligomers allows high yields and easy isolation of the cyclic oliogmers in the AABB- and AB-type polycondensations.

The total macrocyclization was realized by further addition of $TiCl_4$ and 1,4-phenylenediamine during the course of the AABB-type polycondensation of 1,4-dibenzoylbenzene with 1,4-phenylenediamine in the presence of $TiCl_4$. Only peaks attributed to the novel cyclic polyphenylazomethines (CPA*n*-aabb, where *n* is the degree of polymerization) were confirmed in the TOF-MS spectrum of the crude products (Fig. 26). The CPA*n*-aabb products ($n = 4$, 6, 8, 10, 12, 14, 16, 18, and >20) were easily isolated in 13, 23, 16, 11, 8, 6, 5, 3, and 6% yields (total: 91%), respectively, by gel permeation chromatography. Using a similar synthetic procedure, the macrocyclic oligomers, CPA*n*-ab ($n = 3, 4, 5, 6, 7, 8, 9$, and >10), were also isolated in 59, trace, 3, 9, 4, 2, 3, and 4% yields (total: 84%), respectively, in the AB-type polycondensation of 4-amino-4′-bromobenzophenone. The very poor solubility of the conventional PPAs prevents a structural study and their actual application as a polymer material, although all of the obtained macrocycles show a high solubility in chloroform and tetrahydrofuran; therefore, the structural study became feasible.

2.7 *E*/*Z*-Conformation and Regular Molecular-Packing. The obtained macrocycles should have many *E*/*Z* isomers, because they have many imine sites. However, CPA4-aabb, CPA6-ab, and CPA6-aabb were revealed to have only one or a few stable isomers based on their simple ^{13}C NMR spectra. One peak attributed to the azomethine carbon in the spectrum of CPA4-aabb shows that CPA4-aabb has a single isomer with one *Z*-conformation of the azomethine bonds (Fig. 27a). Three peaks attributed to azomethine carbon in the spectrum of CPA6-ab support the C_2-symmetry of an oblong isomer having the *E*/*Z* combination shown in Fig. 27b, and the isomer was also determined by molecular dynamics (MD) calculations as the stable one of CPA6-ab. Two strong peaks and twelve weak ones in the spectrum of CPA6-aabb show that CPA6-aabb has three isomers, i.e., I, II, and III, as shown in Fig. 27c. That is, among the structurally possible *E*/*Z* isomers of CPA6-aabb, only the triangle isomer I gives the two peaks attributed to the azomethine carbon in the spectrum due to its C_3-symmetric structure, and only the asymmetry of isomers II and III results in the six peaks in the spectra. The triangle structure as a stable isomer in CPA6-aabb was also supported by the MD calculations. These results revealed that CPA6-aabb and CPA6-ab, which have the same number of azomethine bonds, have different shapes and *E*/*Z* conformations based on the different linking-patterns (head-to-head or head-to-tail) of the imine bonds.

The X-ray crystal structure of CPA6-aabb clearly supported the structure obtained by NMR and MD calculations. The triangle shape and *E*/*Z* conformations of the crystal molecule agreed with those of isomer I shown in Fig. 27c (Fig. 28a). The phenyl rings shown as "X" in Fig. 28a are parallel to the macrocycle plane, and the phenyl rings shown as "Y" are perpendicular to the macrocycle plane and gather on one side. Interestingly, the triangle molecules have the extremely regular molecular-packing state; they are two-dimensionally packed like the boxing up of "short cakes" (Fig. 28b), and the packed "short cakes" are aligned in a column (Fig. 28c).

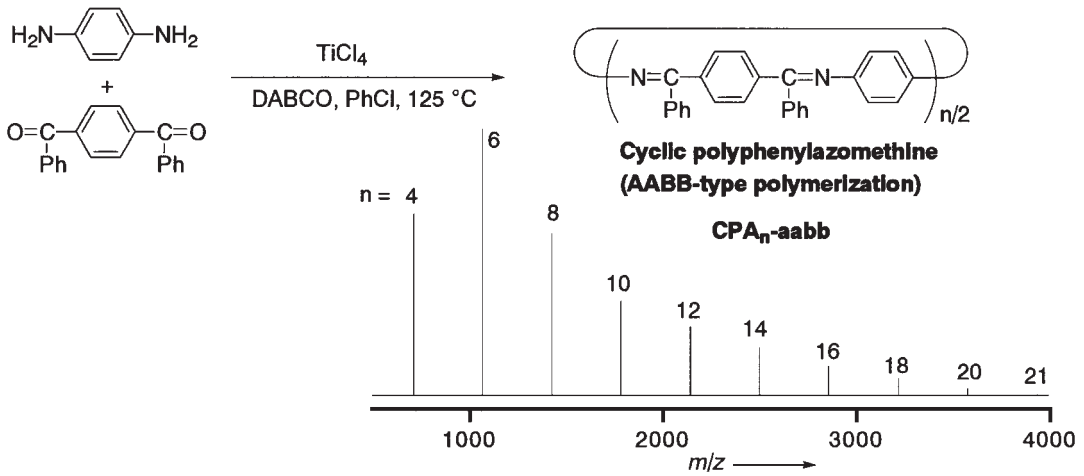

Fig. 26. MALDI-TOF-MS spectrum of CPA*n*-aabb.

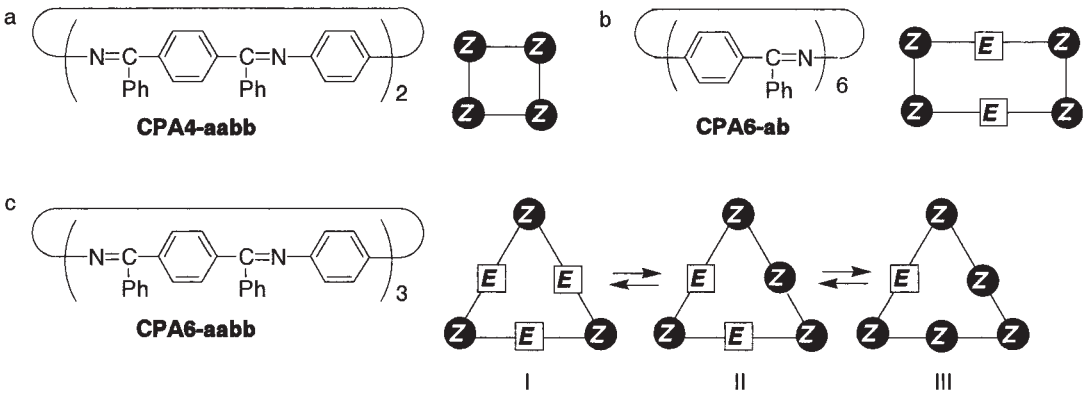

Fig. 27. Shapes and *E*/*Z*-conformations of (a) CPA4-aabb, (b) CPA6-ab, and (c) CPA6-aabb supported by NMR and MD calculations.

2.8 Electrochemical Properties. Linear polyphenylazomethine (PPA) is known to have a poor and unstable redox property due to the easy hydrolysis of the imine bonds and/or further reduction to the amine during the electrochemical measurements in acidic solutions. For example, OPA2′ does not have any redox waves at a potential between −1.0 and 0.0 V, but 2 waves of reduction based on the redox of the imines appeared in the presence of trifluoroacetic acid. This result shows that the redox of OPA2′ occurs at a more positive potential by protonation, and the redox accompanies chemical reduction of the reduced species. On the other hand, CPA*n*-aabb was revealed to have reversible redox-activity in the presence of an acid. The cyclic voltammogram of CPA4-aabb showed two stable redox-waves at a negative potential (Fig. 29). The result of the electrospectrochemical analysis showed the formation of a radical during the first reduction (the decrease of the absorption of azomethine at 400 nm) and the formation of a quinoid during the second reduction (the increase in the absorption at 450 nm). On the basis of the electrospectrochemical analysis and the Nernst plot (slope: −120 and 0 mV/pH, respectively), each redox process was determined to involve a two-electron transfer accompanied by a four-proton transfer and a two-electron transfer per molecule, respectively. The excellent redox properties appear by introduction of a phenyl group at the α-position of the azomethine, which stabilizes both the radical species (Rad) and the quinoidal one (Qn).

Concluding Remarks

Precise control of the number and position of metal ions in the polymer complexes is essential for the development of organic–metallic hybrid nano-materials. We exploited dendritic and cyclic polyphenylazomethines (DPAs and CPAs, respectively) as novel π-cojugated polymer ligands with a single molecular weight and a clearly-defined structure, and we first realized the precise metal-assembling in DPAs based on the unique stepwise complexation behavior. DPAs were synthesized by the convergent method via dehydration of aromatic ketones with aromatic amines in the presence of $TiCl_4$, and showed a high solubility and high thermal stability ($Td_{10\%}$ 521 °C in DPA G4). Based on the conformational rigidity of the π-conjugated backbone, DPA G4 molecules was revealed to have a sphere-like structure (diameter: 2.3 nm) and are regularly assembled on a plate without deformation by means of X-ray crystal analysis, a molecular model, GPC, TEM, AFM, and π–*A* measurements. The stepwise complexation was observed in DPAs as stepwise shifts of the isosbestic point in the UV–vis spectra. DPA G4 has 2, 4, 8, and 16 imine groups in the 1st, 2nd, 3rd and 4th shells, respectively (total, 30 imine groups). DPA G4 can trap 30 equivalents of $SnCl_2$ molecules, because the imine group is complexed with $SnCl_2$ at a ratio of

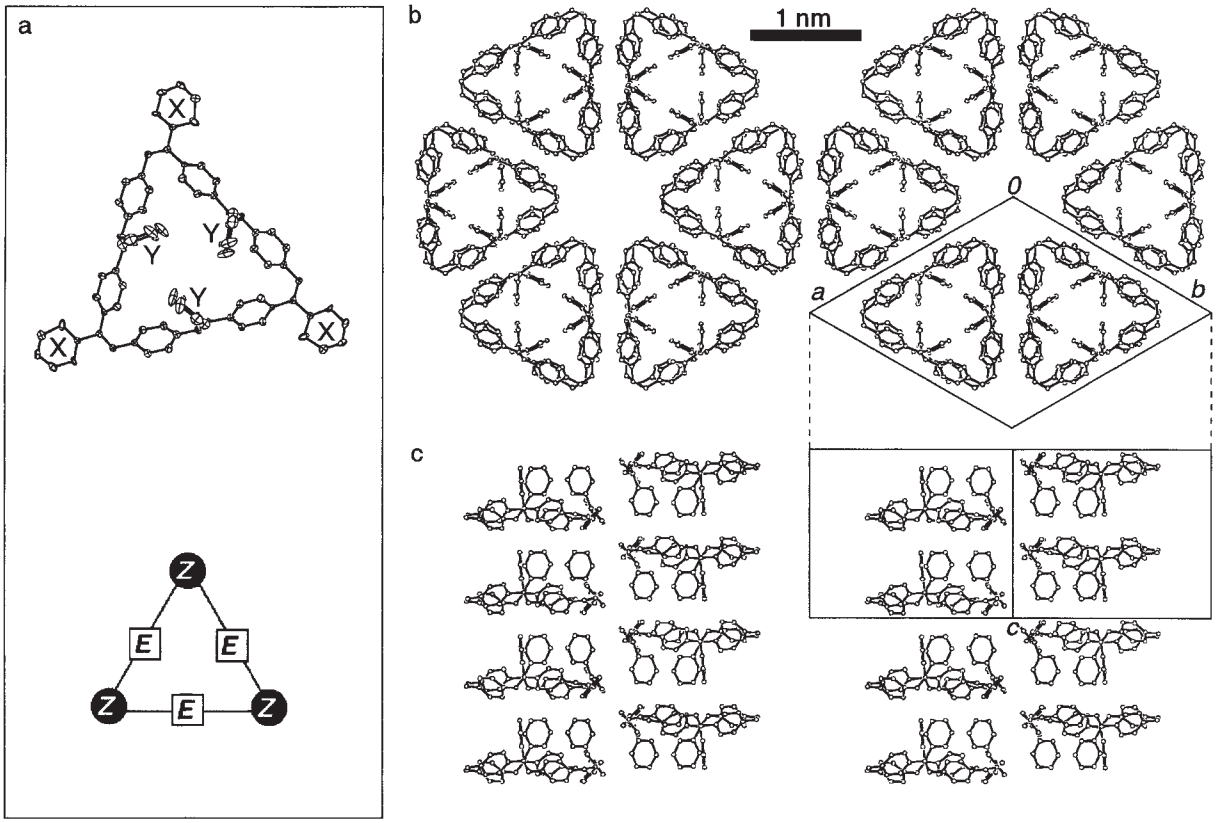

Fig. 28. ORTEP drawing of (a) CPA6-aabb with 20% ellipsoid and the packing structure; (b) top and (c) side views (the phenyl rings shown as "X" in Fig. 28a are omitted for easy understanding of the packing structure).

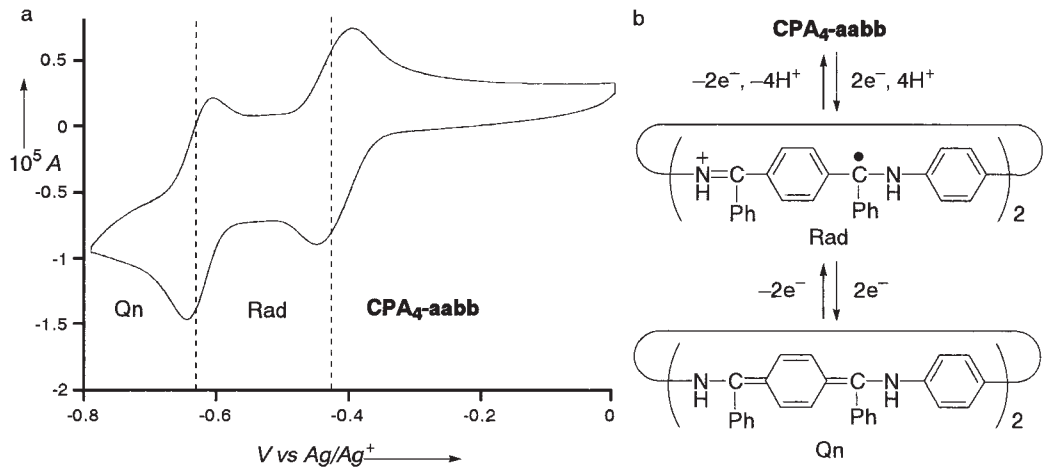

Fig. 29. Cyclic voltammogram of CPA4-aabb (1 mM) in 0.2 M $TBABF_4$/acetonitrile in the presence of trifluoroacetic acid (4 mM) (scan rate = 100 mV/sec; electrode = Pt) and a redox mechanism.

1:1. During addition of 30 equivalents of $SnCl_2$ to DPA G4, four shifts in the isosbestic point were observed in the UV–vis spectra; the amount of $SnCl_2$ added in each step is in agreement with the number of the imine groups in each shell of DPA G4. This result shows that the complexation of the imine groups in DPA G4 with $SnCl_2$ occurs stepwise in the order of the 1st, 2nd, 3rd, and 4th shells. The stepwise complexation was supported by TEM, NMR, and a novel shell-selective reduction (SSR) method for imines. The stepwise complexation is caused by the different basicity of the imine groups between the shells, which was supported by the chemical shifts of the peaks attributed to the imine carbons in the ^{13}C NMR spectra. In addition, the gradients in the basicity were controlled by the introduction of electron-withdrawing or -releasing groups to the core of the dendrimers; the core imines were complexed last in DPAs having a 2,3,5,6-tetrafluoro- or 2,5-dichlorophenyl core due to the low basicity of the core imines.

On the other hand, we established the selective synthesis of CPAs, and found redox activation of CPAs based on the complexation. CPAs were synthesized in a one-step dehydration of

4-aminobenzophenones in the presence of $TiCl_4$ or *p*-toluenesulfonic acid (PTS), and isolated in over 90% yield under non-dilute conditions. When using $TiCl_4$ as the dehydration agent, the introduction of bulky substituents at the α-position of the substrate enhanced the yields of the CPAs. PTS served as an effective catalyst for the synthesis of the phenyl-substituted CPA. This different reactivity between $TiCl_4$ and PTS depends on the dehydration mechanism being dominated by a kinetic process or a thermodynamic one. The structures of the obtained CPAs were confirmed by the NMR, UV–vis spectra, and the result of a MM2 calculation to have only a *Z* conformation and a non-conjugated structure compared to the linear oligophenylazomethines (OPAs). Controlled cyclization was applied for dendrimer synthesis, and a novel dendrimer with a cyclic structure was quantitatively obtained via controlled cyclization on the basis of a steric effect using a monomer with a bulky dendron. Cyclization in hyperbranched polymer synthesis was first controlled on the basis of a steric effect using a Lewis acid with a bulky ligand. Only phenylazomethine oligomers having a cyclic structure were formed during the polymerization of 4,4′-diaminobenzophenone in the presence of $TiCl_4(THF)_2$ as a Lewis acid with bulky ligands. The structure of a cavity in an isolated cyclic oligomer was determined by X-ray crystal analysis. Highly preferential formation of CPA*n* was achieved by further addition of $TiCl_4$ and/or the monomer during the course of the polycondensation. All of the obtained macrocycles show a high solubility unlike the conventional linear polyphenylazomethines. NMR, MD calculations, X-ray crystal analysis, and CV measurements revealed their unique structures based on the *E*/*Z* conformation of the azomethine bonds, the extremely regular molecular-packing state, and the reversible redox-activity by protic acid doping.

This work was partially supported by a Grant-in-Aid for priority area and for Scientific Research from the Ministry of Education Science Foundation Culture, and a Grant-in-Aid for Evaluative Technology from the Science and Technology Agency, and by a Kanagawa Academy Science and Technology (KAST) Research Grant.

References

1 Organic–metallic (inorganic) hybrid nano-materials, see: a) C. Q. Liu, J. B. Lambert, and L. Fu, *J. Am. Chem. Soc.*, **125**, 6452 (2003). b) D. J. Maxwell, J. R. Taylor, and S. M. Nie, *J. Am. Chem. Soc.*, **124**, 9606 (2002). c) S. Inagaki, S. Guan, T. Ohsuna, and O. Terasaki, *Nature*, **416**, 304 (2002). d) Y. F. Lu, Y. Yang, A. Sellinger, M. C. Lu, J. M. Huang, H. Y. Fan, R. Haddad, G. Lopez, A. R. Burns, D. Y. Sasaki, J. Shelnutt, and C. J. Brinker, *Nature*, **410**, 913 (2001). e) E. Coronado, J. R. Galan-Mascaros, C. J. Gomez-Garcia, V. Laukhin, *Nature*, **408**, 447 (2000). f) R. P. Kingsborough and T. M. Swager, *J. Am. Chem. Soc.*, **121**, 8825 (1999).

2 π-Conjugate polymers, see: "Handbook of Organic Conductive Molecules and Polymers," ed by H. S. Nalwa, Wiley-VCH, New York (1997), Vol. 1–5.

3 a) K. Yamamoto, M. Higuchi, H. Takai, and T. Nishiumi, *Org. Lett.*, **3**, 131 (2001). b) K. Yamamoto, M. Higuchi, K. Uchida, and Y. Kojima, *Macromolecules*, **35**, 5782 (2002). c) T. Nishiumi, M. Higuchi, and K. Yamamoto, *Macromolecules*, **36**, 6325 (2003).

4 π-Conjugated polymer–metal complexes, see: a) M. Higuchi, D. Imoda, and T. Hirao, *Macromolecules*, **29**, 8277 (1996). b) M. Higuchi, I. Ikeda, and T. Hirao, *J. Org. Chem.*, **62**, 1072 (1997). c) M. Higuchi and T. Hirao, *Kobunshi Ronbunshu*, **54**, 632 (1997).

5 Dendrimers, see: a) "Supramolecular Polymers," ed by A. Ciferri, M. Dekker, New York (2000). b) "Dendrimer I, II, III," ed by F. Vögtle, Springer, New York (2001). c) "Dendrimer and Dendrons," ed by G. R. Newkome, C. N. Moorefield, and F. Vögtle, Wiley-VCH, New York (2001). d) D. A. Tomalia, J. Dewald, M. Hall, S. Martin, and P. B. Smith, *Prepr. SPSJ Int. Polym. Conf.*, 1st, 65 (1984). e) D. A. Tomalia, H. Baker, and J. R. Dewald, *Polym. J.*, **17**, 117 (1985). f) G. R. Newkome, Z. Q. Yao, G. R. Baker, and V. K. Gupta, *J. Org. Chem.*, **50**, 2003 (1985). g) D. A. Tomalia, A. M. Naylor, and W. A. Goddard, III, *Angew. Chem., Int. Ed. Engl.*, **29**, 138 (1990). h) A. W. Bosman, H. M. Janssen, and E. W. Meijer, *Chem. Rev.*, **99**, 1665 (1999). i) M. Fischer and F. Vögtle, *Angew. Chem., Int. Ed.*, **38**, 884 (1999). j) S. M. Grayson and J. M. J. Fréchet, *Chem. Rev.*, **101**, 3819 (2001).

6 Energy transfer in dendrimers, see: a) C. Devadoss, P. Bharathi, and J. S. Moore, *J. Am. Chem. Soc.*, **118**, 9635 (1996). b) D. L. Jiang and T. Aida, *Nature*, **388**, 454 (1997). c) T. D. Selby and S. C. Blackstock, *J. Am. Chem. Soc.*, **120**, 12155 (1998).

7 Dendrimer–metal complexes, see: a) L. Balogh and D. A. Tomalia, *J. Am. Chem. Soc.*, **120**, 7355 (1998). b) M. Zhao, L. Sun, and R. M. Crooks, *J. Am. Chem. Soc.*, **120**, 4877 (1998). c) R. M. Crooks, M. Zhao, L. Sun, V. Chechik, and L. K. Yeung, *Acc. Chem. Res.*, **34**, 181 (2001). d) M. Tominaga, J. Hosogi, K. Konishi, and T. Aida, *Chem. Commun.*, **2000**, 719. e) D. J. Díaz, G. D. Storrier, S. Bernhard, K. Takada, and H. D. Abruña, *Langmuir*, **15**, 7351 (1999). f) M. Petrucci-Samija, V. Guillemette, M. Dasgupta, and A. K. Kakkar, *J. Am. Chem. Soc.*, **121**, 1968 (1999). g) M. Kawa and J. M. J. Fréchet, *Chem. Mater.*, **10**, 286 (1998). h) G. R. Newkome, E. He, and C. N. Moorefield, *Chem. Rev.*, **99**, 1689 (1999). i) D. Astruc and F. Chardac, *Chem. Rev.*, **101**, 2991 (2001). j) V. Balzani, P. Ceroni, A. Juris, M. Venturi, S. Campagna, F. Puntoriero, and S. Serroni, *Coord. Chem. Rev.*, **219**, 545 (2001).

8 Macrocycles with π-conjugated backbones, see: a) D. Zhao and J. S. Moore, *J. Org. Chem.*, **67**, 3548 (2002). b) S. Lahiri, J. L. Thompson, and J. S. Moore, *J. Am. Chem. Soc.*, **122**, 11315 (2000). c) Y. Tobe, N. Utsumi, K. Kawabata, A. Nagano, K. Adachi, S. Araki, M. Sonoda, K. Hirose, and K. Naemura, *J. Am. Chem. Soc.*, **124**, 5350 (2002). d) J. R. Nitschke, S. Zürcher, and T. D. Tilley, *J. Am. Chem. Soc.*, **122**, 10345 (2000). e) Y. Tain, J. Tong, G. Frenzen, and J. Sun, *J. Org. Chem.*, **64**, 1442 (1999).

9 Polyphenylazomethines, see: a) R. Adams, R. E. Bullock, and W. C. Wilson, *J. Am. Chem. Soc.*, **45**, 521 (1923). b) C. S. Marvel and N. W. Hill, *J. Am. Chem. Soc.*, **72**, 4819 (1950). c) C. S. Marvel and N. Tarköy, *J. Am. Chem. Soc.*, **79**, 6000 (1957). d) C. S. Marvel and N. Tarköy, *J. Am. Chem. Soc.*, **80**, 832 (1958). e) C. S. Marvel and P. V. Bonsignore, *J. Am. Chem. Soc.*, **81**, 2668 (1959). f) L. G. Kaufman, P. T. Funke, and A. A. Volpe, *Polym. Prepr. (Am. Vhem. Soc. Div. Polym. Chem.)*, **11**, 250 (1970). g) A. A. Volpe, J. C. Carson, Jr., and L. G. Kaufman, *Thermochim. Acta*, **2**, 175 (1971). h) K. Suematsu, K. Nakamura, and J. Takada, *Polym. J.*, **15**, 71 (1983). i) P. W. Morgan, S. L. Kwolek, and T. C. Pletcher, *Macromolecules*, **20**, 729 (1987). j) C. J. Yang and S. A. Jenekhe, *Chem. Mater.*, **3**, 878 (1991). k) S. A. Jenekhe, C. J. Yang, H. Vanherzeele, and J. S. Meth, *Chem. Mater.*, **3**, 985 (1991). l) C. J. Yang and S. A. Jenekhe, *Supramolecular Sci.*, **1**, 91 (1994). m) C. J. Yang and S. A. Jenekhe, *Macro-*

molecules, **28**, 1180 (1995). n) O. Thomas, O. Inganäs, and M. R. Andersson, *Macromolecules*, **31**, 2676 (1998).

10 Dendritic polyphenylazomethines, see: a) M. Higuchi, S. Shiki, and K. Yamamoto, *Org. Lett.*, **2**, 3079 (2000). b) M. Higuchi, S. Shiki, K. Ariga, and K. Yamamoto, *J. Am. Chem. Soc.*, **123**, 4414 (2001). c) K. Yamamoto, M. Higuchi, S. Shiki, M. Tsuruta, and H. Chiba, *Nature*, **415**, 509 (2002). d) M. Higuchi and K. Yamamoto, *J. Synth. Org. Chem., Jpn*, **60**, 869 (2002). e) M. Higuchi, M. Tsuruta, H. Chiba, S. Shiki, and K. Yamamoto, *J. Am. Chem. Soc.*, **125**, 9988 (2003).

11 Cyclic polyphenylazomethines, see: a) M. Higuchi and K. Yamamoto, *Org. Lett.*, **1**, 1881 (1999). b) M. Higuchi, A. Kimoto, S. Shiki, and K. Yamamoto, *J. Org. Chem.*, **65**, 5680 (2000). c) M. Higuchi, H. Kanazawa, M. Tsuruta, and K. Yamamoto, *Macromolecules*, **34**, 8847 (2001). d) M. Higuchi and K. Yamamoto, *Polym. Adv. Technol.*, **13**, 765 (2002). e) M. Higuchi, H. Kanazawa, and K. Yamamoto, *Org. Lett.*, **5**, 345 (2003).

12 Syntheses of polyphenylazomethines using *p*-toluenesulfonic acid, see: T. Miyaji, C. Azuma, E. Asaoka, and S. Nakamura, *J. Polym. Sci., Part A: Polym. Chem.*, **38**, 1064 (2000).

13 Molecular-assembling of dendrimers, see: a) A. Hierlemann, J. K. Campbell, L. A. Baker, R. M. Crooks, and A. J. Ricco, *J. Am. Chem. Soc.*, **120**, 5323 (1998). b) H. Tokuhisa, M. Zhao, L. A. Baker, V. T. Phan, D. L. Dermody, M. E. Garcia, R. F. Peez, R. M. Crooks, and T. M. Mayer, *J. Am. Chem. Soc.*, **120**, 4492 (1998). c) J. Li, D. R. Swanson, D. Qin, H. M. Brothers, L. T. Piehler, D. Tomalia, and D. T. Meier, *Langmuir*, **15**, 7347 (1999).

14 Characterization of hyperbranched polymers, see: a) P. J. Flory, *J. Am. Chem. Soc.*, **74**, 2718 (1952). b) A. Morikawa, M. Kakimoto, and Y. Imai, *Macromolecules*, **25**, 3247 (1992). c) D. Yu, N. Vladimirov, and J. M. J. Fréchet, *Macromolecules*, **32**, 5186 (1999).

15 Complexation of $SnCl_2$ with imines, see: J. M. Van den Berg, *Acta Crystallogr.*, **15**, 1051 (1962).

16 Cyclic aromatic oligomers, see: a) W. Memeger, Jr., J. Lazar, D. Ovenall, and R. A. Leach, *Macromolecules*, **26**, 3476 (1993) (cyclic aramids). b) K. P. Chen, Y. Wang, and A. S. Hay, *Macromolecules*, **28**, 653 (1995) (cyclic aryl ether ketones). c) K. P. Chan, Y.-F. Wang, A. S. Hay, X. L. Hronowski, and R. J. Cotter, *Macromolecules*, **28**, 6705 (1995) (cyclic aryl ether ketones). d) Y. Ding and A. S. Hay, *Macromolecules*, **29**, 6386 (1996) (cyclic aromatic disulfides). e) H. Jiang, T. Liu, H. Zhang, T. Chen, and Z. Mo, *Polymer*, **37**, 3427 (1996) (cyclic aryl carbonates). f) H. M. Colquhoun, D. F. Lewis, R. A. Fairman, I. Baxter, and D. J. Williams, *J. Mater. Chem.*, **7**, 1 (1997) (cyclic aryl thioether ketones). g) J. Wang, C. Chen, X. Xun, S. Wang, and Z. Wu, *J. Polym. Sci., Part A: Polym. Chem.*, **37**, 1957 (1999) (cyclic aryl ether ketones).

17 Dendrimer synthesis via cyclization, see: a) S. Hecht and J. M. J. Fréchet, *J. Am. Chem. Soc.*, **121**, 4084 (1999). b) S. C. Zimmerman, F. Zeng, D. E. C. Reichert, and S. V. Kolotuchin, *Science*, **271**, 1095 (1996). c) V. Percec, W. Cho, G. Ungar, and D. J. P. Yeardley, *Angew. Chem., Int. Ed.*, **39**, 1597 (2000).

18 Cyclization during hyperbranched polymerization, see: a) A. Burgath, A. Sunder, and H. Frey, *Macromol. Chem. Phys.*, **201**, 782 (2000). b) J. K. Gooden, M. L. Gross, A. Mueller, A. D. Stefanescu, and K. L. Wooley, *J. Am. Chem. Soc.*, **120**, 10180 (1998). c) D. Parker and W. J. Feast, *Macromolecules*, **34**, 2048 (2001). d) P. Bharathi and J. S. Moore, *Macromolecules*, **33**, 3212 (2000).

Masayoshi Higuchi was born in 1969 in Niigata, Japan. He received his degrees of B. Eng. (1993), M. Eng. (1995), and Dr. Eng. (1998) from Osaka University. He was appointed as a Research Associate of Keio University in 1998, and promoted to an Assistant Professor in 2003. During 1995–1998, he was a Research Fellow of the Japan Society for the Promotion of Science for Young Scientists (JSPS Research Fellow). During 2001–2004, he is also an investigator in the Kanagawa Academy of Science & Technology (KAST). He received the Chemical Society of Japan Award for Young Chemists for 2002. His current research is focused on organic–metallic hybrid nanomaterials using novel topological π-conjugated supramolecules.